Volume 62
Number 10
5 February 2026
Pages 3063–3392

ChemComm

Chemical Communications

rsc.li/chemcomm

ISSN 1359-7345

ROYAL SOCIETY OF CHEMISTRY

HIGHLIGHT

Kwan Woo Nam *et al.*

Interfacial design strategies using metal–organic frameworks: a comprehensive review for rechargeable batteries

ChemComm

HIGHLIGHT

View Article Online
View Journal | View Issue

Cite this: *Chem. Commun.*, 2026, **62**, 3077

Interfacial design strategies using metal–organic frameworks: a comprehensive review for rechargeable batteries

Jinyoung Lee, †[a] Yoonjin Oh, †[a] Yunsu Ahn †[ab] and Kwan Woo Nam *[ab]

Received 15th September 2025,
Accepted 2nd January 2026

DOI: 10.1039/d5cc05318h

rsc.li/chemcomm

Modifying battery interfaces to improve stability and performance, and suppress side reactions has been a long-standing goal. Although there were many candidates, metal–organic frameworks (MOFs) have garnered particular attention owing to their unique porous structure, tunability, and multifunctionality. Due to these characteristics, MOFs could contribute to regulating the diffusion path of carrier ions, mitigating undesired reactions, as well as stabilizing the interfaces. Therefore, MOFs were increasingly explored as functional layers and host materials for lithium-ion, lithium–metal, lithium–sulfur, and aqueous zinc-ion batteries. However, challenges remained regarding their structural stability, compatibility, and scalability under realistic operating conditions. This review aimed to highlight critical side reactions at the interface, summarized previous research efforts addressing these issues, and offered promising strategies for further development.

1. Introduction

Since the commercialisation of rechargeable batteries in the 20th century, extensive efforts have been focused on increasing their energy density, cycle-life, and operating voltage. Several successful studies were conducted before this review, with results such as lithium-ion batteries (LIBs) attaining a high theoretical capacity of 3860 mAh g^{-1} and long-life span,[1] but several critical challenges remain. Although they vary depending on the type of battery, side reactions such as dendrite formation, electrode corrosion, and electrolyte decomposition remain unsolved, leading to severely reduced performance, efficiency, and safety risks. These issues primarily originate from interfacial degradation.[2] Therefore, understanding how side reactions at the interfaces of each battery's components occur and modifying them are crucial.

Rechargeable batteries consist of four main components: cathode, anode, separator, and electrolyte. This review discusses the problems occurring at the three interfaces of the four core battery components: cathode–electrolyte, separator–electrolyte, and anode–electrolyte (Fig. 1). In the cathode–

[a] *Department of Chemical Engineering and Materials Science, and Graduate Program in System Health Science and Engineering, Ewha Womans University, Seoul 03760, Republic of Korea. E-mail: leejinyoungace@ewhain.net, fabulus@ewhain.net, emma4864@ewhain.net, kwanwoo@ewha.ac.kr*
[b] *Institute for Multiscale Matter and Systems (IMMS), Ewha Womans University, Seoul 03760, Republic of Korea*
† These authors contributed equally to this work.

Jinyoung Lee

Jinyoung Lee received her BS degree in Chemical Engineering and Materials Science from the Ewha Womans University. Her research interests focus on interfacial engineering for rechargeable batteries using metal–organic frameworks and biomimetic amphiphilic systems to stabilize aqueous zinc anodes.

Yoonjin Oh

Yoonjin Oh received her BS degree in Chemical Engineering and Materials Science from the Ewha Womans University. Her research interests focus on zinc interfacial engineering in aqueous zinc-ion batteries using MOF-based materials.

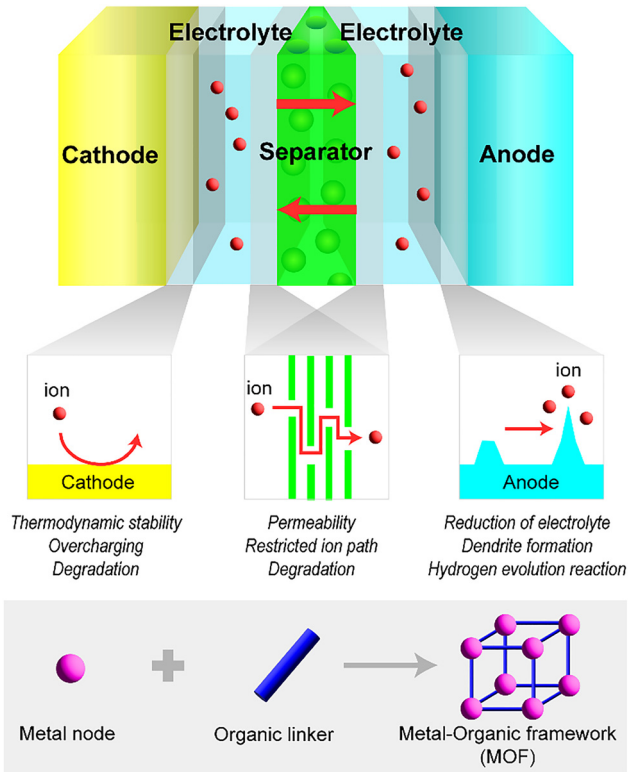

Fig. 1 Schematic illustration of interfacial issues in battery components (cathode, anode, and separator) with MOF structure.

electrolyte interface (CEI), the thermodynamic stability of the electrolyte and cathode gradually decreases as the cycle increases.[3] Also, overcharging of the cathode causes oxidation of the electrolyte, leading to a decrease in cell performance and life span. Likewise, at the anode–electrolyte interface, electrolyte reduction and dendrite formation remain major challenges. In aqueous zinc-ion batteries (AZIBs), the hydrogen evolution reaction (HER) and electrode corrosion also occur as side reactions at the interface. Although the separator–electrolyte interface does not directly suffer from side reactions like dendrite formation, the permeability of carrier ions is largely dependent on the affinity between the electrolyte and the separator. In addition, the side reactions occurring at electrode interfaces, such as dendrite and electrolyte decomposition during overcharging, cause degradation of the separator, which leads to a reduction in cell performance and efficiency.[4]

An interface regulation method was proposed to solve the problems mentioned above. There are several successful material candidates for interface regulation, including inorganic, polymer, carbon based, and metal–organic framework (MOF) based materials. Inorganic materials such as Al_2O_3,[5] TiO_3,[6] and ZrO_2[7] have been actively investigated. However, the inorganic-based materials suffer from a lack of ionic conductivity and structural vulnerability. On the other hand, polymer-based materials such as polyethylene oxide (PEO),[8] polyvinylidene fluoride (PVDF),[9] and other conducting polymers,[10] have amazing flexibility and tunability which makes them promising candidate materials. However, their major disadvantages include extremely low thermal and chemical stability, along with potential unsuitability for electrode modification considering their oxidation potential. Carbon-based materials such as graphene[11] and carbon nanotubes[12] tend to exhibit excellent electrical conductivity and chemical stability as well. Yet, challenges remain due to the insufficient effect on overall electrode modification.[13]

MOFs are also frequently used as interface modification agents to improve cell performance. A MOF is a three-dimensional (3D) porous crystal consisting of metal nodes and organic ligands. Its unique tunability in terms of composition and pore size allows various separations such as gas/liquid phase separation and capturing organic molecules and ions from solution.[14,15] The use of a MOF as an intermediate layer between interfaces enables suppression of side reactions and improves the cell's overall performance regardless of the type of battery.

Recently, MOFs have been widely explored for interface modification. For example, applying a redox-active MOF on the cathode of lithium sulfur batteries (LSBs) could improve the energy density of pouch cells up to 316.5 Wh kg^{-1}.[16] When the

Yunsu Ahn

Yunsu Ahn received her BS degree in Chemical Engineering and Materials Science from the Ewha Womans University. Her research interests focus on MOF-based cathode materials for aqueous zinc-ion batteries and superionic conductors for all-solid-state batteries.

Kwan Woo Nam

Kwan Woo Nam is currently an Assistant Professor in the Department of Chemical Engineering and Materials Science at the Ewha Womans University, South Korea. He received his PhD degree in EEWS in 2016 from KAIST. His current research includes the mechanistic analysis of new cathodes for multivalent batteries and designing functional materials to increase performance for separators, binders, and electrodes in rechargeable batteries.

anodes of LIBs were modified by a bimetallic NiCo-MOF material, the specific capacity after 200 cycles remained relatively high at 696.3 mAh g^{-1}.[17] Also, when a separator of AZIBs was modified using NM-125, a capacity retention rate of 99.8% was achieved.[4]

This review discusses cell performance and efficiency improvements induced by MOF-applied interface regulation. Previous studies are categorized based on the battery components modified by MOFs—cathode, anode, separator—and further classified by the battery type, including conventional LIBs and next-generation batteries such as LSBs or lithium metal batteries (LMBs) and AZIBs.

2. Cathode modification using MOFs

For the development of high-performance batteries, it is essential to deeply understand the reactivity at the cathode–electrolyte interface and its impact on overall performance and stability (Fig. 2a). To address these CEI problems, a range of strategies utilizing MOFs are currently emerging (Fig. 2b and c). Attempts to utilize MOFs as interfacial coatings on cathode materials face several practical challenges.[18,19] Microcrystalline domains within MOFs hinder the formation of uniform and conformal coating layers, while excessively thick MOF layers can obstruct charge transport, thereby reducing the volumetric energy density of the cell. Furthermore, the intrinsically low ionic conductivity of MOFs increases interfacial resistance, limiting their effectiveness as coating materials. As a result, research on MOF-based cathode interface coatings remains limited. In contrast, strategies that employ MOF-derived composites as cathode active materials have attracted considerable attention due to their potential to enhance electrochemical performance.[20] Therefore, this review focuses on recent progress in the development of MOF-derived composites as cathode active materials, highlighting their potential contributions to improving electrochemical characteristics.

There is a growing demand for high-energy-density LIBs with high operating voltage and large capacity. One effective strategy to enhance the energy density of LIBs is to increase the cut-off voltage.[21] However, increasing the cut-off voltage accelerates the interfacial reaction between the cathode and the electrolyte, which may lead to rapid capacity loss or cell failure.

A typical LSB consists of a lithium (Li) metal anode, an organic liquid electrolyte, a separator, and a sulfur based cathode, in which elemental sulfur—commonly in the orthorhombic α-S_8 form—is embedded within a conductive carbon framework.[22] LSBs are considered one of the most promising candidates to replace LIBs because of their theoretically high energy density, low cost, and the environmental benignity of sulfur. Nevertheless, the cell level operational performance of LSBs has yet to meet the requirements for practical implementation. One of the most fundamental issues lies in the unstable electrochemical reactions occurring at the cathode–electrolyte interface. Another critical challenge is the degradation of active materials at the cathode–electrolyte interface during cycling. A highly conductive and thermodynamically stable CEI is crucial for enhancing the cycle life of the LSBs.

AZIBs are considered a promising alternative to LIBs for grid and off-grid applications owing to their rechargeability, cost-effectiveness, and the high theoretical volumetric energy density of the zinc (Zn) metal anode.[23,24] However, the large ionic radius of the hydrated Li^+ ($\sim$4.7 Å) leads to strong electrostatic interactions between the inserted charge carriers and the host cathode structure, resulting in sluggish diffusion kinetics and poor rate performance.[25] In addition, the desolvation process at the electrode–electrolyte interface has also emerged as a critical challenge. For hydrated Zn ions to be inserted into the cathode, the surrounding water molecules must be removed through desolvation first. However, this process requires high activation energy, hindering the efficient insertion of Zn^{2+}.

2.1. Modification of LIB cathodes using MOFs

The development of MOF-derived cathode materials provides structural and morphological tunability that can effectively address the inherent limitations of conventional cathodes, such as limited energy density, and short cycle life. Framework materials like MOFs have the essential properties needed for use as surface modifiers in electrochemical applications. In particular, they offer the following advantages:[26]

(i) High porosity and large specific surface area.

(ii) Tunable physical and chemical properties.

(iii) Efficient charge transport through uniform pores and channels.

These features make them highly advantageous for the surface modification of commercial cathode materials in LIBs. Moreover, surface modification of commercial cathode materials using MOFs or MOF-derived materials has attracted considerable attention as a promising strategy to enhance structural stability and electrochemical performance during battery cycling.

J. Lin *et al.*[27] developed an *in situ* synthetic strategy to form a MOF-derived carbon-encapsulated $LiCoO_2$ (LCO) heterostructure *via* high-temperature solid-state annealing. In this approach, ZIF-67 (ZIF = zeolitic imidazolate framework), a cobalt (Co)-containing MOF, was used as the precursor and transformed into LCO particles through high-temperature calcination followed by lithiation. The resulting carbon coating layer stabilized the LCO/electrolyte interface by preventing direct contact, enhancing electron transport, and alleviating structural strain during Li^+ insertion/extraction. As a result, the nitrogen (N)-doped LCO@C-700 electrode exhibited an extended cycle life and remarkable electrochemical performance, maintaining a gravimetric/areal capacity of 171.1 mAh g^{-1}/4.2 mAh cm^{-2} after 200 cycles at 1C, and delivering 150.3 mAh g^{-1} even at 10C.

To address the issues of low initial coulombic efficiency (ICE) and poor stability of Li-rich Mn-based oxides, C. Huang *et al.*[28] proposed a ZIF-67-derived coating strategy to construct a Co_xO_y/C composite layer on the $Li_{1.2}Mn_{0.54}Ni_{0.13}Co_{0.13}O_2$ (LRMO) surface through MOF self-assembly followed by heat treatment. This Co_xO_y/C coating layer effectively blocked direct contact between the electrolyte and the electrode, thereby

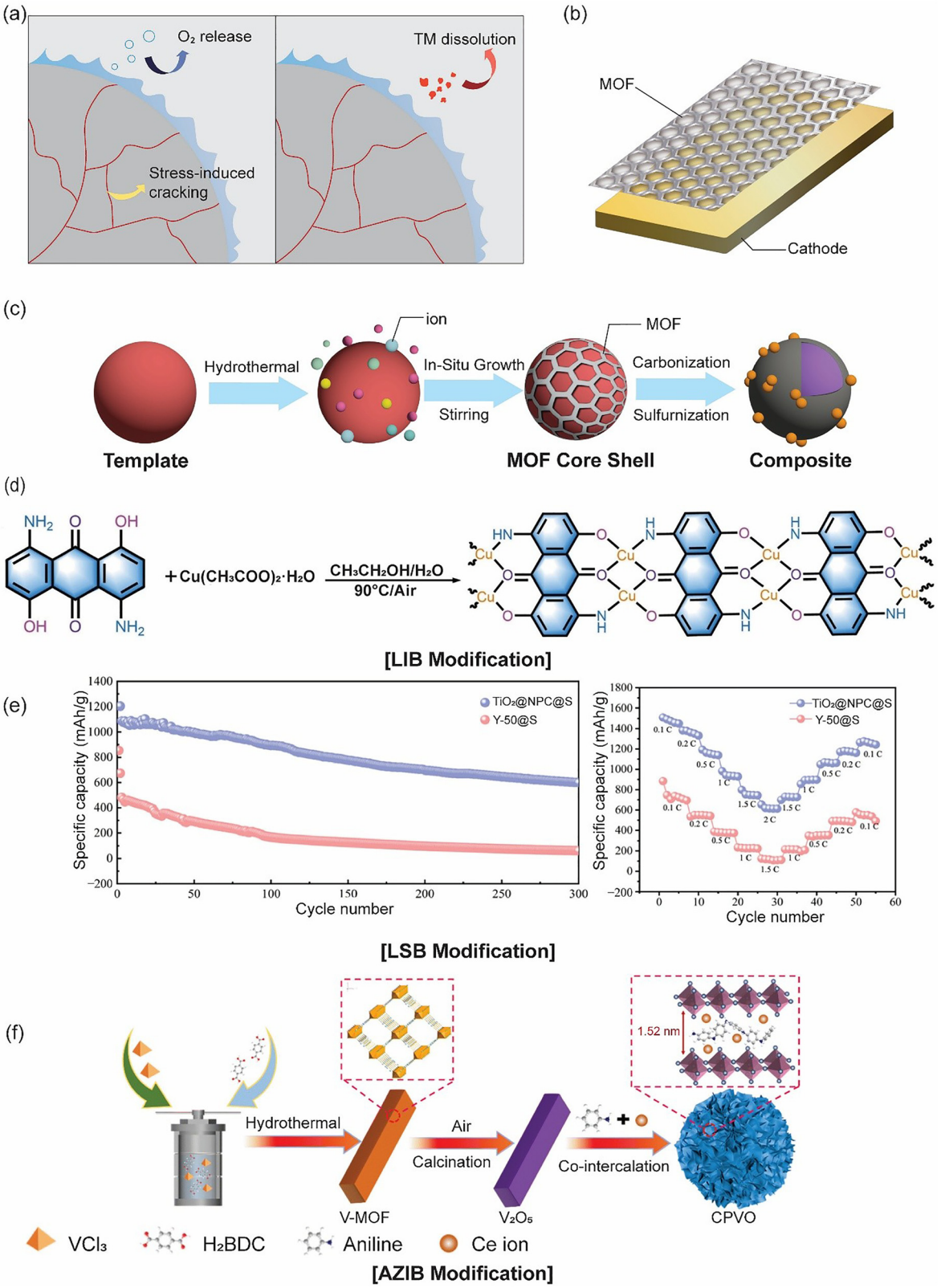

Fig. 2 (a) Schematic illustration of side reactions that could occur in CEI. (b) Scheme of modifying CEI using the MOF coating strategy. (c) Scheme of modifying CEI using the MOF-derived composite strategy. (d) Synthetic schematic diagram of DDA–Cu in LIB. Adapted from ref. 32 with permission from Angewandte Chemie International Edition, Copyright 2025. (e) Cycle-life performance and rate performance of TiO_2@NPC@S in LSB. Adapted from ref. 36 with permission from Carbon Future, Copyright 2025. (f) Schematic illustration of the formation process of CPVO nanosheets in AZIB. Adapted from ref. 44 with permission from the Royal Society of Chemistry.

suppressing CEI formation. It also prevented corrosion of the LRMO surface. It also effectively suppressed O^{2-} loss in the lattice after electron depletion and mitigated side reactions between surface O^{n--} species and the electrolyte, thereby promoting a reversible anionic redox process. After three initial activation cycles at 0.1C, the LRMO@Co_xO_y/C electrode exhibited a high ICE of 91.5%, with a charge capacity of 289.1 mAh g^{-1} and a discharge capacity of 264.6 mAh g^{-1}. Furthermore, after 150 cycles, it maintained a reversible capacity of 194.2 mAh g^{-1} with a capacity retention rate of 80.2%.

Z. Wu *et al.*[29] synthesized a highly redox-active two-dimensional (2D) MOF named Cu-BHT, $[Cu_3(C_6S_6)]_n$, using Cu(II) salt and benzenehexathiolate (BHT) as precursors. The BHT ligand coordinates with the d^9 Cu(II) ion to form a –Cu–S– kagome lattice structure. This structure enabled high redox reversibility, resulting in a high electrical conductivity of 231 S cm^{-1}. As a cathode material, Cu-BHT delivered an outstanding reversible capacity of 175 mAh g^{-1} at 300 mA g^{-1} and showed an extremely low-capacity degradation rate of only 0.048% per cycle over 500 cycles. It also maintained high-rate capabilities, retaining most of its capacity at elevated current densities.

S. Shin *et al.*[30] proposed a Li-insertion-type metal–organic framework (i-MOF) coating on $LiNi_{1-x-y}Co_xMn_yO_2$ (NCM) to enhance ion transport and stabilize the cathode–electrolyte interface. The i-MOF interfacial layer suppressed undesirable side reactions at the CEI, mitigated particle cracking, and inhibited transition-metal dissolution. The i-MOF-coated sample referred to as i-NCM, exhibited excellent electrochemical performance, delivering high discharge capacities of 219.87 mAh g^{-1} at 0.1C and 203.53 mAh g^{-1} at 1C. Also, it showed markedly improved capacity retention under harsh conditions (50 °C), confirming the effectiveness of the i-MOF layer in protecting the cathode surface from electrolyte-induced degradation.

Cu-MOF materials possess significant potential as cathodes for LIBs due to their excellent electrical conductivity and high structural tunability.[31] However, their practical application has been hindered by limitations in capacity and cycling stability. M. Yang *et al.*[32] reported a one-dimensional (1D) DDA–Cu (DDA = 1,5-diamino-4,8-dihydroxy-9,10-anthracenedione, Cu = Copper) featuring extended π-d conjugated coordination nanoribbons and high-density redox-active centers, enabling both high capacity and long-term electrochemical stability in LIBs. The 1D conductive DDA–Cu MOF was synthesized *via* a coordination reaction between $Cu(CH_3COO)_2{\cdot}H_2O$ as the metal source and DDA as the organic ligand (Fig. 2d). DDA–Cu exhibited a high electrical conductivity of 1.63×10^{-4} S cm^{-1} compared to traditional MOFs and high thermal stability up to 320 °C. As a cathode, DDA–Cu delivered a high reversible capacity of 353 mAh g^{-1} at 50 mA g^{-1} and demonstrated outstanding cycling stability with 78% capacity retention after 1000 cycles.

These papers demonstrated a common interfacial design principle: either inhibiting direct contact with the electrolyte and unfavorable side reactions through the MOF coating layer or maximizing charge transport dynamics by promoting ion and electron movement, thereby imparting active reactivity and catalytic functionality. Notably, the integration of artificial-intelligence (AI)-driven design will particularly accelerate the discovery of advanced MOF structures. AI can be employed in the predictive optimization of key structural parameters (such as metal node selection, linker functionalization, and defect generation) that govern ion transport and interfacial stability. Rather than relying on iterative trial and error, AI models can rapidly scan the chemical space, identify optimal compositions, and propose experimentally feasible coating conditions, thereby shortening development time. With the continued expansion of the electric vehicle and grid-scale storage markets, these chemically tunable, computationally guided MOF coatings will play a pivotal role in next-generation battery technology, with commercialization anticipated within the next decade.

2.2. Modification of next-generation battery cathodes using MOFs

LSBs possess a high theoretical energy density, making them strong candidates for next-generation batteries.[33] However, their practical application is hindered by several challenges, including the shuttle effect of lithium polysulfide (LiPS), the dendrite formation of Li metal anodes, and the volumetric expansion of sulfur cathodes. To overcome these issues, MOFs have attracted significant attention due to their outstanding adsorption and catalytic properties, as well as their easily tunable structural flexibility.

Y. Feng *et al.*[34] reported a Cu-based metal–organic framework (CuMOF) host that chemically immobilized sulfur in LSBs. The CuMOFs were synthesized *via* a solution-based coordination reaction using Cu salts and benzene-1,3,5-tricarboxylic acid as the organic ligand. Sulfur introduced by melt diffusion formed CuMOF–S composites with enhanced interfacial stability. Moreover, the CuMOF host effectively stabilized more than 19.3 wt% of sulfur, mitigating polysulfide (PS) dissolution during prolonged cycling and substantially enhancing coulombic efficiency (CE). Among the various CuMOF–S composites, the CuMOF1S2 cathode (with a CuMOF-to-S ratio of 1 : 2) delivered an excellent capacity retention of 1051.3 mAh g^{-1} over 300 cycles at a current density of 200 mA g^{-1}, demonstrating remarkable electrochemical stability. These findings underscored the potential of CuMOFs as chemically interactive hosts for high performance sulfur cathodes in LSBs.

Y. Xie *et al.*[35] synthesized a MOF-derived $Co_{0.85}Se$/NC composite by embedding $Co_{0.85}Se$ nanoparticles within nitrogen-doped carbon (NC) nanosheet arrays grown on a carbon cloth (CC) substrate. This hierarchical structure offered a high specific surface area and porosity, thereby providing abundant active sites for LiPS conversion and effectively mitigating the volume expansion during charge/discharge cycles. The $Co_{0.85}Se$ nanoparticles served as polar adsorption centers and electrocatalysts, accelerating LiPS redox kinetics. $Co_{0.85}Se$/NC can maintain a discharge capacity of 678 mAh g^{-1} at a high sulfur loading of 4.08×10^{-3} g cm^{-2} even after 50 cycles at 0.1C. The $Co_{0.85}Se$/NC-S cathode exhibited outstanding cycling stability

over 400 cycles, while delivering high discharge capacities of 1001 mAh g^{-1} at 1C.

Q. Zeng *et al.*[16] proposed a strategy for the rational design and implementation of a redox-active metal–organic framework (RM-MOF) that can simultaneously function as a sulfur host and redox mediator (RM). As a precursor, MIL-101(Cr) (MIL: Materials from Institute Lavoisier) was first synthesized, and dithiothreitol (DTT) was selected as the redox-active unit. Based on this design, terminal water molecules on MIL-101(Cr) were removed under high vacuum and elevated temperature, and DTT molecules were chemically anchored onto the exposed octahedral trinuclear $Cr(III)_3O$ building units, thereby forming the RM-MOF. The resulting RM-MOF exhibited an excellent discharge capacity of 883.6 mAh g^{-1} at 3C and achieved over a 90% reduction in capacity decay during long-term cycling. Furthermore, the RM-MOF enabled practical operation of pouch cells even under high sulfur loading conditions, delivering an impressive energy density of 316.5 Wh kg^{-1}.

P. Shi *et al.*[36] developed a 3D MOF-derived hierarchical porous TiO_2@NPC@S composite (NPC = nanoporous carbon). The TiO_2@NPC@S composite was prepared *via* MOF carbonization followed by sulfur melt diffusion. The MOF-derived TiO_2@NPC preserved a 3D pill-like architecture with hierarchical pores, providing sufficient space for sulfur accommodation and effective confinement within the framework. Benefiting from this hierarchical conductive–polar hybrid architecture, the TiO_2@NPC@S cathode delivered an initial discharge capacity of 1327.35 mAh g^{-1} at 0.5C and maintained a low average capacity fading rate of 0.18% per cycle after 300 cycles (Fig. 2e). Furthermore, it demonstrated outstanding rate performance, achieving 928 mAh g^{-1} at 1C and 743 mAh g^{-1} at 1.5C, confirming the significant enhancement in electrochemical performance enabled by the MOF-derived TiO_2@NPC@S structure.

MOF-based cathodes for LSBs demonstrate exceptional capabilities in suppressing the PS shuttle effect, enabling high areal capacities of up to 13.8 mAh cm^{-2} and energy densities reaching 316.5 Wh kg^{-1} under high sulfur loading conditions.[16] The design of electrically conductive metal–organic frameworks (c-MOFs) and the optimization of their large scale synthesis often require substantial computational resources and involve considerable complexity.[37]

To overcome these limitations, machine learning (ML) and AI are expected to play a pivotal role. For example, ML models can rapidly screen viable metal–ligand combinations from large datasets, predict electronic conductivity pathways, and map structure–property relationships. AI-based generation and optimization algorithms can propose new c-MOF structures, support inverse design, and recommend synthesis conditions that maximize crystallinity and conductivity. Taken together, AI can generate and optimize new c-MOF design concepts, while ML can rapidly evaluate their structural feasibility and predicted properties, enabling the identification of promising candidates computationally before experimental validation.

With $3.5 billion in funding allocated by the U.S. Department of Energy, commercialization efforts are rapidly accelerating, with pilot-scale pouch cell validation anticipated between 2025 and 2027. In the long term, the integration of MOFs with solid-state electrolytes, and real-time monitoring technologies is expected to enable next-generation battery architectures. These technological advancements are poised to position MOF-enabled LSBs as core enablers in aerospace, electric mobility, and grid-scale energy storage systems by the 2030s.

AZIBs are emerging as a next-generation energy storage technology, offering notable advantages in terms of safety and rate performance compared to LIBs. K. W. Nam *et al.*[38] employed a 2D c-MOF, $Cu_3(HHTP)_2$, (HHTP = hexahydroxytriphenylene), featuring large 1D nanorods with channels, as the cathode material. This structure enabled the direct insertion of hydrated Zn^{2+} into the host framework, resulting in fast ion diffusion and low interfacial resistance. $Cu_3(HHTP)_2$ followed an intercalation pseudocapacitance mechanism, exhibiting redox reactions at approximately 1.06 V and 0.88 V *versus* Zn/Zn^{2+}. The electrode delivered a reversible capacity of 228 mAh g^{-1} at 50 mA g^{-1} and retained 75% of its capacity (124.4 mAh g^{-1}) after 500 cycles at 4000 mA g^{-1}. These results highlighted the excellent rate capability and cycling stability of $Cu_3(HHTP)_2$ as a promising Zn battery cathode.

In AZIBs, manganese (Mn) based cathode materials are commonly employed due to their abundance and cost-effectiveness. However, their practical application is hindered by rapid capacity fading and poor rate performance, mainly caused by Mn dissolution and disproportionation reactions.

To overcome these limitations, C. Yin *et al.*[39] successfully synthesized hierarchical spheroidal MnO@C composites using Mn-based MOFs as precursors. During thermal conversion, the Mn-BTC precursor transformed into MnO spheres assembled into short nanorods, while simultaneously forming a uniform carbon coating on the particle surface. The MnO–C heterointerface effectively suppressed Mn ion dissolution and enhanced structural stability. When applied as a cathode material for AZIBs, the MnO@C composite exhibited outstanding electrochemical performance, delivering an excellent rate capability of 165.9 mAh g^{-1} at a high current density of 3000 mA g^{-1}, and maintaining a stable capacity of 160 mAh g^{-1} even after 1000 cycles under the same conditions. Furthermore, at a low current density of 100 mA g^{-1}, the electrode achieved a high specific capacity of 412.4 mAh g^{-1}.

W. Wang *et al.*[40] fabricated MOF-derived (Zn,Mn)S/C-coated heterogeneous microspheres ((Zn,Mn)S/C@MnS) through an *in situ* growth and thermal treatment process. Dodecahedral ZIF-8 particles were grown *in situ* on the surface of spherical manganese carbonate to obtain ZIF-8@$MnCO_3$ microspheres. Subsequent carbonization and sulfurization converted these microspheres into MOF-derived (Zn,Mn)S/C-coated manganese-sulfide heterogeneous structures ((Zn,Mn)S/C@MnS). This architecture exhibited excellent rate capability and outstanding cycling stability. The (Zn,Mn)S/C@MnS electrode delivered a high initial discharge capacity of 374.1 mAh g^{-1} at a current density of 200 mA g^{-1}, and maintained a capacity of 226.5 mAh g^{-1} with a CE of 99.23% after 100 cycles. Moreover, it retained 85.6 mAh g^{-1} even after 1000 cycles at a high current density of 1000 mA g^{-1},

demonstrating excellent long-term durability. These results confirmed that the MOF-derived (Zn,Mn)S/C heterostructure effectively enhanced interfacial stability and charge-transfer kinetics.

M. Jiang *et al.*[41] synthesized a MOF-derived ZnO–$ZnMn_2O_4$ (MZ) composite enriched with oxygen vacancies (O_V). By tuning the calcination temperature, the optimized MZ-550 formed uniform spherical particles with abundant oxygen vacancies, which enhanced electronic conductivity and reaction kinetics. Benefiting from these defect-engineered interfaces and the stabilizing role of ZnO, MZ-550 demonstrated a high specific capacity of 314.5 mAh g^{-1} at a current density of 100 mA g^{-1}. Even under a high current density of 1000 mA g^{-1} it retained 96.6% of its maximum capacity after 1600 cycles at 1000 mA g^{-1}. Furthermore, the material maintained high capacities of 86.4 mAh g^{-1} at −20 °C and 331.1 mAh g^{-1} at 40 °C, highlighting its excellent electrochemical performance under extreme temperature conditions.

Vanadium (V) based cathodes, despite their high capacity,[42] are constrained by a low operating voltage. To overcome this limitation, D. Jia *et al.*[43] synthesized a MIL-88B(V)@rGO composite by anchoring MIL-88B(V) nanorods onto reduced graphene oxide (rGO) sheets *via* a simple hydrothermal method. Graphene oxide played a key role in controlling the crystal growth of MIL-88B(V), promoting the formation of nanoscale rod-shaped structures. During the initial charge/discharge cycle, MIL-88B(V) underwent an *in situ* electrochemical oxidation into amorphous V_2O_5, which then functioned as the electrochemically active material for the subsequent reversible Zn^{2+} intercalation and deintercalation. The amorphous V_2O_5 provided abundant ion transport pathways and active sites for rapid Zn^{2+} diffusion. The rGO sheets facilitated continuous electron and ion transport, thereby accelerating redox reactions and enhancing pseudocapacitive behavior. The MIL-88B(V)@rGO cathode delivered a high discharge capacity of 479.6 mAh g^{-1} at 50 mA g^{-1} and exhibited excellent rate capability, retaining a capacity of 263.6 mAh g^{-1} even at a high current density of 5000 mA g^{-1}. Furthermore, it demonstrated outstanding electrochemical stability, retaining 80.3% of its capacity after 400 cycles at 2000 mA g^{-1}.

Commercial V_2O_5 suffers from inherent limitations, including its low specific surface area, nonporous structure, poor intrinsic conductivity, and narrow interlayer spacing, which collectively result in limited active sites, sluggish ion transport, and slow electrode kinetics. Y. Zhang *et al.*[44] synthesized a novel cathode material: cerium (Ce) and polyaniline (PANI) co-intercalated V-MOF-derived porous V_2O_5 nanosheets (denoted as CPVO) *via* a simple hydrothermal method (Fig. 2f). The resulting CPVO exhibited a high specific surface area and a nanosheet-like porous morphology, which collectively offered abundant Zn^{2+} diffusion pathways and electrochemical active sites. These features significantly increased ion diffusion kinetics and enable high-capacity performance. As a result, CPVO delivered an impressive specific capacity of 498.5 mAh g^{-1} at a current density of 100 mA g^{-1}, while maintaining a high-rate performance of 385.6 mAh g^{-1} at 5000 mA g^{-1}.

X. Wu *et al.*[45] developed a hierarchical $V_2O_3/V_3O_5/Zn_2VO_4$@NC composite (denoted as ZnVO-800) through a self-sacrificial reaction between the ZIF-8 precursor and NH_4VO_3. The resulting ZnVO-800 retained the polyhedral morphology of ZIF-8 and formed a heterojunction architecture embedded in N-doped carbon, which shortened ion-diffusion pathways and increased the CEI area. Upon initial discharge at a current density of 500 mA g^{-1}, the ZnVO-800 cathode delivered a high reversible capacity of 314.0 mAh g^{-1}. Notably, it retained a reversible capacity of 100.1 mAh g^{-1} with 90.8% capacity retention even after 3000 cycles, demonstrating excellent long-term cycling stability.

X. Ma *et al.*[46] fabricated ultrathin vanadium oxide nanosheets (C@V_2O_3@C) encapsulated within dual carbon layers *via* a stepwise MXene-to-MOF conversion strategy. Initially, V_2CT_x MXene was transformed into C@V_2O_3 nanosheets, followed by an *in situ* conversion into a V_2O_3-derived MOF, and ultimately subjected to carbonization to form the final composite. The resulting C@V_2O_3@C architecture exhibited a large specific surface area, abundant porosity, a high V_2O_3 content, and ultrathin inner and outer carbon matrix. These structural features enhanced charge-transfer kinetics, increased active surface area, and effectively suppressed V dissolution during cycling. C@V_2O_3@C exhibited nearly 100% capacity retention at a current density of 1000 mA g^{-1} and maintained a discharge capacity of 240 mAh g^{-1} even after 3000 cycles at a high current density of 30 000 mA g^{-1}. In particular, it delivers an excellent rate performance, with a discharge capacity of 402 mAh g^{-1} under the extreme condition of 50 000 mA g^{-1}.

Research on MOF-based cathode engineering for AZIBs has evolved along three primary directions: optimizing electrochemical reaction mechanisms, enhancing structural stability, and improving ion diffusion pathways through various MOF structures and derivatives. Early efforts focus on 2D c-MOFs that exhibit supercapacitor-like charge storage behavior. Subsequently, a hybrid design incorporating carbon coatings, sulfides, and oxides effectively suppresses active material dissolution and extends the cycle life. More recently, the limits of material performance have been expanded by simultaneously increasing O_V and electronic conductivity *via* defect engineering. Looking forward, future advances are expected to focus on: (1) integrated architecture combining gel or solid-state hydrated aqueous electrolyte and MOF cathode, aiming to concurrently improve both safety and energy density; (2) intelligent MOF frameworks with dynamic defect generation capabilities to maximize cyclability. Such integrated innovations will not only accelerate the commercialization of AZIBs but also lay the groundwork for next-generation grid-scale energy storage systems (ESSs).

3. Anode modification using MOFs

At the anode–electrolyte interface, the formation of a solid electrolyte interphase (SEI) is essential. The reduction of electrolyte solvent at the anode interface causes decomposition of electrolyte, which forms the SEI layer. This layer conducts ions, blocks electrons, and varies with thetype and structure of the electrolyte and anode.[47] Consequently, the ability to regulate the formation and stability of the SEI plays a pivotal role in

advancing cell performance. Several points are required at the anode–electrolyte interface to improve battery performance, lifespan, and reduce safety risks. According to a comprehensive review of the SEI layer by K. Xu, the main influencing factors can be summarized as follows.[48] The battery's overall performance will be improved:

(i) As the chemical composition of the SEI layer has good chemical and thermal stability. This reduces the instability of the battery under high-temperature conditions.

(ii) As the structural uniformity of the SEI layer increases. This enhances the desolvation process of the carrier ion.

(iii) As the mechanical stability of the SEI layer is increased. This enables the SEI layer to better withstand the anode's volume changes during cycling.

Recently, MOFs used for interface modification have been extensively studied. Unlike cathode or separator interface modification using MOFs as the precursor or derivative, most of the anode modifications are mainly about coating MOFs on the anode interface. This is because the application strategy and structural requirements vary for different areas of application. For anodes, it is important to stabilize the SEI and mitigate volume expansion, so MOFs are commonly used as surface coating agents. In contrast, the cathode and separator generally have low interfacial reactivity and deformation. Therefore, MOFs are used as precursors to enhance cell performance.[49,50]

3.1. Modification of LIB anodes using MOFs

There are two widely used anode materials for LIBs: carbon-based and silicon (Si) based anodes. They both suffer from non-uniform SEI layer formation during battery cycling. These non-uniform SEI formations can cause anode volume change, capacity fading, and safety issues.[51] In particular, Si anodes have a higher theoretical capacity of 4200 mAh g^{-1}, which is 11 times higher than carbon-based anodes.[52] However, it undergoes a dramatic volume change of up to 300%, which significantly reduces cell capacity and stability.

These problems could be addressed by modifying the electrolyte–anode interface using MOFs. However, most of the MOFs used in the modification of LIB anodes (especially for carbon-based anodes), use MOFs as a 'precursor'. This is because the porous structure of MOFs ensures efficient storage capacity and ion conductivity when carbonized under high temperature conditions. For example, S. Mamidi *et al.*[53] used ZIF-67 to immerse the 3D carbon micro electrode and then calcined it at 350 °C, forming a modified carbon-based anode: 3DCGS-Co. The cobalt oxide petals in 3DCGS-Co provided conductive pathways that reduced anode resistance and facilitated Li^+ diffusion, increasing capacity through conversion redox reactions.

Therefore, 3DCGS-Co exhibited an enhanced capacity retention rate of 88.9% after 200 cycles, as well as a CE of 99%. Moreover, the electrode recovered a capacity of 1036 mAh g^{-1} when cycled at 50 mA g^{-1}, indicating the outstanding rate reversibility and structural robustness of the modified anode.

Also, recent investigations tend to focus on using MOFs as precursors for more precise and advanced carbon-based anodes. Y. Yang *et al.*[54] used Co-doped MOFs as a precursor to make Co–ZnO/C as well as Co–Co_3O_4/C nanohybrids, which performed as an excellent anode for LIBs. Co–Co_3O_4/C was made by calcination of the Co-doped MOF, thereby it consisted of abundant pores that ensured the Li-ion diffusion as well as a large surface area. Therefore, the MOF-modified anode showed a highly reversible capacity of 898 mAh g^{-1} (0.1C current density after 100 cycles). Also, its CE gradually reached 100% as the cycle proceeded. These superior results stemmed from using the MOF as a precursor, which formed mesoporous structures that regulated volume expansion and enabled fast ion-electron transport.

On the other hand, MOFs were also applied in the modification of Si-based anodes. A variety of methods could be used when modifying the electrolyte-anode interface to enhance battery performance. Y. Han *et al.*[55] used the sandwich coating method MOF (MOF-SC) to modify the anode interface. MOF particles were cast onto the surface of a nano- or micro-Si layer above the super P to improve cycling performance. The bottom layer (super P) improved electrical contact, the middle layer (Si) acted as a Li storage material, and the top layer (MOFs) enabled fast diffusion of electrolyte as well as reduced exposure of Si. By this, the cycling capacity was remarkably improved, without noticeable areal capacity fading after 100 cycles, maintaining 600 μAh cm^{-2}, whereas pristine nano-Si exhibited nearly complete capacity loss within 50 cycles. This research played a major role in anode interface modification because it suggested not only the type of MOF that exhibited good performance, but also the efficient structure for coating the anode interface, which could be applied using different MOFs.

L. Zhang *et al.*[56] used ZIF-67 as a MOF precursor to enhance cell stability and capacity. Si nanoparticles used for the anode material were evenly coated with ZIF-67, which uses Co metal nodes and 2-methylimidazole linkers. By heating this at 800 °C, organic linkers of ZIF-67 were carbonized to form a modified anode with a porous characteristic shell. These shells made significant improvements: inhibited anode volume expansion, enhanced electrical conductivity, and allowed interface stabilization by preventing direct contact between the electrolyte and Si anode. The improvement made could also be quantitatively measured. After interface modification, not only the ICE increased by 50.8% to 72.0% but also showed a fabulous capacity retention rate after 500 cycles of 73.1% (at 0.5C and 60 °C).

Recently, Y. Y. Chen *et al.*[57] used silane/MOF as a precursor to make SiO_x/Co@C (pore size of 1.7 to 36.2 nm) for an anode coating agent. This work overcame the limitations of existing methods: the difficulty of forming strong bonds between Si and MOFs. This was because MOFs were used as self-sacrificing templates to firmly encapsulate SiO_x by deriving Co embedded in the carbon framework. More specifically, this MOF-derived structure promoted uniform distribution, prevented agglomeration, and mechanically stabilized the anode during cycling. Furthermore, single-atom Co sites catalysed Si–O bond conversion, enhancing reversibility and reaction kinetics. For example, SiO_x/Co@C-600 showed only 24.6% of the volume expansion rate, whereas SiO_x@C (bare anode) showed 88.6%

of the expansion rate after 600 cycles (Fig. 3a). This control of anode volume change enabled improvement in conductivity and battery performance. After interface modification, not only did the ICE increase by 42.9% to 78.9% but also a significant long-term cycling capacity (reversible capacity of 815.5 mAh g^{-1} after 240 cycles at 100 mA g^{-1}) was observed.

Overall, electrolyte–anode modification using MOFs showed excellent potential in improving LIB stability as well as electrochemical performance. Unique characteristics of versatile MOFs such as tunability and porosity, provided improved ion transport paths, enhanced capacity, and volume change mitigation. Recent investigations have actively researched regulating distinctive side reactions in batteries using new MOF architectures, techniques such as thermal/hydrothermal treatment, hybrid structures such as sandwich-like or nano structures, and so on. Ultimately, integrating carbon- and Si- based anodes with MOFs through precise structural and technical control may be the key strategy for achieving high capacity and stable LIBs.

3.2. Modification of next generation battery anodes using MOFs

LMBs use Li metal as an anode material. Li metal has a high theoretical capacity and negative potential of 3860 mAh g^{-1} and −3.04 V (relative to the standard hydrogen electrode). This enables the design of high-energy and power batteries, which is the main reason why LMBs are gaining significant attention as the next-generation battery.[58,59] However, the two main problems hinder the commercialisation of LMBs (Fig. 3b). As the charging/discharging process proceeds, the rapid formation of dendrites occurs at the anode interface. Hence, electrically isolated dead Li and repetitive SEI layer formation occur continuously, which ultimately leads to low CE of LMB. These issues can potentially lead to internal shorts and safety issues, as well as shorten the cycle life of the battery.[60,61]

As with LIBs, the stated problems can be addressed through interface modifications using MOFs. Artificial SEI layer, MOFs in this case, could potentially block electrolyte contact from the electrode, reduce cell overpotential, as well as enhance single-ion conductivity. However, there are plenty of things to consider: SEI layers made by MOFs are usually poor conductors. Therefore, modifying the interface by maximizing the porosity of MOFs to provide efficient ion transport channels without negatively affecting the conductivity is the main issue. To achieve these goals, MOF modification using plating or electrochemical deposition strategies is commonly used.[62]

T. Zhou *et al.*[63] used Co-MOF to modify the Li metal anode. A 2D Co-MOF was synthesized and annealed on CC, forming CC@CN–Co, changing lithiophobic CC into a lithiophilic framework. Then electrochemical deposition of Li metal on CC@CN–Co took place to finally make the 3D CC@CN–Co@Li composite. Through a unique synthesis strategy, the CC@CN–Co@Li composite has evenly distributed N containing functional groups and Co nanoparticles, which allowed the modified anode to have uniform Li nucleation and inhibit the formation of dendrites. Also, nanosheet arrays and binder-free structures formed by a direct growing process enabled enhancement of active surface area and reduced the 'dead mass' of the anode. These features allowed excellent cycling performance at relatively high current conditions as well as a stable CE of 98.7% for nearly 300 cycles (Fig. 3c). Furthermore, it exhibited stable cycling performance while maintaining a low overpotential of 20 mV throughout more than 800 cycles. Such electrochemical advantages originated from the CC@CN–Co@Li composite having dendrite-free features and a highly stable electrolyte-anode interface.

Recent research tended to take more specific and unique approaches to interface modifications. For example, J. Ding *et al.*[64] used the 'glass state' MOF to modify the electrolyte-anode interface: ZIF-62 glass, by far the most studied ZIF glass was used. ZIF-62 features Zn nodes linked by imidazole and benzimidazole ligands arranged in a tetrahedral geometry. The ZIF-62 crystals were first synthesized using a hydrothermal method, followed by a melt quenching process to finally form the ZIF-62 glass. Then, ZIF-62 glass was chopped down and made into slurry, which was directly coated onto Cu foil using the doctor-blade method. Afterwards, electrochemical deposition of Li metal took place, finally forming Li@glass@Cu. ZIF-62 glass enabled Li@glass@Cu to regulate Li deposition through its unique features as the 'glass state': isotropic and internal grain-boundary-free characteristics (Fig. 3d). Therefore, Li@glass@Cu exhibited uniform Li-ion diffusion indicating the absence of dendrite formation and the fast diffusion process due to its isotropic structure. This was demonstrated by symmetric and full cell performance experimental results. The full cell (Li@glass@Cu||LFP) was shown to exhibit a relatively higher capacity of 148 mAh g^{-1} compared to that of Li@Cu||LFP of 131 mAh g^{-1}. Moreover, Li@glass@Cu||LFP possessed excellent cycling stability and showed capacity retention up to 90% at 1C, 1000 cycles.

Another recent study used a quasi-2D fluorinated carbonized MOF (q2D-FcMOF) to form the artificial SEI layer. L. Kong *et al.*[65] used four kinds of MOFs (ZIF-8, ZIF-67, UIO-66, and Ni-MOF) which underwent a similar process of ice-templating, carbonization, and fluorination, forming each q2D-FcZ8, q2D-FcZ67, q2D-FcU66, and q2D-FcNiMOF. These q2D-FcMOFs were suspended in droplets that were cast and evaporated on Li metal, creating a dense and uniform coating, finally forming q2D-FcMOF@Li electrode. Particularly, q2D-FcMOF formed a robust artificial SEI layer, which has an inner layer mainly composed of inorganic LiF which is lithiophobic, as well as an outer layer mainly composed of metal ion clusters that are lithiophilic. Therefore, the inner layer inhibited side reactions and dendrite growth, while the outer layer improved the mechanical stability of the SEI. This dual-layer architecture enabled efficient Li^+ conduction and uniform nucleation at the interface. Through this, the overall battery's charge/discharge kinetics became harmonious, leading to enhancement in the battery's performance and stability. For example, a symmetrical q2D-FcZ8@Li cell exhibited a low overpotential of 44 mV and long cycling life of 3600 h. Additionally, the q2D-FcZ8@Li||LFP full cell showed excellent capacity retention of 92.85% over 600

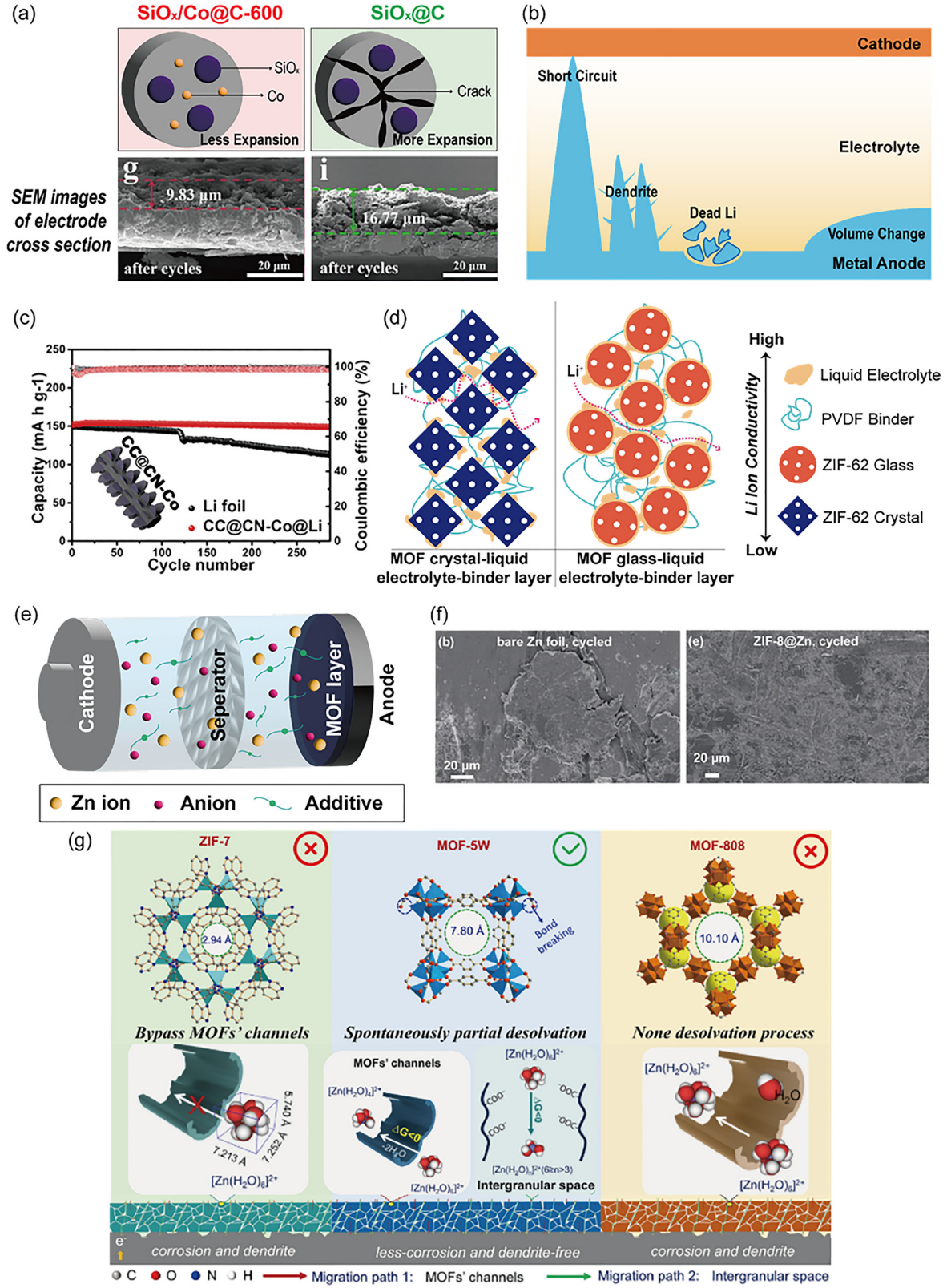

Fig. 3 (a) Scheme and SEM images of cycled electrode cross section of SiO_x/Co@C-600 and SiO_x@C in LIBs. Adapted from ref. 57 with permission from Chemical Engineering Journal, Copyright 2025. (b) Crucial side reactions that occur in the anode-electrolyte interface of LMB. (c) Long cycling performance of CC@CN–Co@Li|| LFP@C and Li||LFP@C full cells at 5C in LMBs. Adapted from ref. 63 with permission from Advanced Functional Materials, Copyright 2025. (d) Scheme of Li ion migration at crystal and glass MOF conditions in LMBs. (e) Scheme of MOF modified AZIBs. (f) SEM images of bare Zn and ZIF-8@Zn after cycling. Adapted from ref. 79 with permission from Nanomicro Letters, Copyright 2025. (g) Scheme of migration of hydrated Zn^{2+} with different pore size MOFs in AZIBs. Adapted from ref. 70 with permission from Energy Storage Materials, Copyright 2025.

cycles with an ultrahigh CE of 99.71%. Although q2D-FcZ8@Li produced the best results, other q2D-FcMOFs@Li (q2D-FcZ67@Li, q2D-FcU66@Li, and q2D-FcNiMOF@Li) showed surprisingly improved results compared to the bare Li electrode.

In summary, unique characteristics of MOFs—such as their tunability, porosity, versatility, and functionality—enabled cell performance enhancement *via* homogeneous Li nucleation, provided an effective ion movement path, and improved interfacial stability. While recent studies tend to focus on more specific and unique approaches, challenges remain in translating lab-scale improvement plans to a commercial scale. Nevertheless, since coating techniques are more commonly applied than the heat treatment ones in LMB modification, it is thought that LMB commercialization of surface modification using MOFs will be somewhat easier than LIBs.

AZIBs have gained significant attention as a cost-efficient next-generation battery because Zn metal is cheaper than Li metal and water-based electrolytes are more eco-friendly and safer than organic electrolytes (Fig. 3e).[76] However, there are critical side reactions, especially at the anode interface that degrade cell performance and stability. One of the critical side reactions occurring at the anode interface is Zn dendrite formation. Notably, AZIBs exhibit much severe dendrite formation than LIBs, due to the high mechanical rigidity of Zn metal and other side reactions such as the HER in aqueous environments.[77] By this, as the charge/discharge cycle repeats, Zn ions tend to accumulate in specific regions due to the tip effect, which ends up forming dendrite growth. Another major side reaction is the HER. At the anode-electrolyte interface, the Zn anode and H_2O solvent used in the electrolyte undergo a reduction reaction, resulting in evolution of hydrogen gases. Furthermore, corrosion of the Zn metal may occur.[78] These side reactions may deteriorate capacity, efficiency, and stability of AZIBs.

Critical side reactions mentioned above can also be controlled by interface modification using MOFs. Among all the other types of batteries (LIBs, LMBs, *etc.*), AZIBs have attracted the most attention with regard to interface modification using MOFs. This is mainly because the vulnerabilities of AZIBs and the strengths of MOF are well-matched, creating harmonious synergy. More specifically, the critical challenges of Zn anode instability in AZIBs can be improved *via* the unique porous structure, catalytic effect of metal nodes, and suppression of electrolyte decomposition by organic ligands. These improvements synergistically enhance the electrochemical performance of AZIBs without compromising their inherent advantages, such as low cost and high safety. For these reasons, a variety of prior research has been conducted using various types and structures of MOFs (Table 1).

X. Pu *et al.*[79] proposed full battery component innovation using MOFs. AZIBs proposed in the paper used a Mn(BTC) MOF cathode, ZIF-8 coated anode, and $ZnSO_4$ as the electrolyte to finally enable high performance ESS. ZIF-8 was coated on Zn foil forming an interface modified anode (ZIF-8@Zn), which eventually showed 8 times longer cycle life compared to bare Zn. This was because not only did ZIF-8's unique porous structure lead to homogenization of the Zn ion flux, but it also provided a stable interface that suppressed dendrite formation and reduced interfacial resistance. Therefore, the surface of ZIF-8@Zn remained very clear compared to bare Zn which exhibited large protuberances/dendrites even after 100 cycles (Fig. 3f). Also, the ZIF-8@Zn symmetric cell exhibited good cycling stability of over 170 h at 0.25 mA cm^{-2}, 0.05 mAh cm^{-2} conditions. Overall, the proposed fully improved cell showed excellent long-term cycling stability of 92% capacity retention after 900 cycles at 1000 mA g^{-1}.

Y. Xiang *et al.*[75] used amorphous MOF (A-MOF) as a flexible protective layer on a Zn metal anode. Through the steric hindrance effect of acetate ion, crystallization of ZIF-8 was suppressed, eventually forming an amorphous structured MOF (A-ZIF-8). A-ZIF-8 had unique characteristics such as enhanced flexibility and bonding force, as well as reduced defects and grain boundaries, due to the amorphous structure. These characteristics guaranteed excellent improvement on mechanical properties, interfacial properties, and electrochemical

Table 1 Recent studies of electrolyte–anode interface modifications using MOFs (C1, C2, and C3 are each condition for overpotential and cycling performance measurements, each having [mA cm^{-2}], [mA cm^{-2}], and [mAh cm^{-2}])

Type	MOFs	Method	Electrolyte	Nucleation overpotential (C^1)	Cycling performance (C^2, C^3)	Average CE	Ref.
Surface coating	ZIF-8	Mechanical coating and infiltration	3 M $Zn(CF_3SO_3)_2$	15.2 mV (1)	800 h (1, 1)	~99.6%	66
	2D ZIF-8	Mechanical coating	2 M $ZnSO_4$	20 mV (1)	3000 h (1, 1)	99.4%	67
	Zn/Cu-MOF (ZCM)	Mechanical coating	3 M $Zn(CF_3SO_3)_2$	23.9 mV (5)	1082 h (2, 1)	~99.0%	68
	Ce–Fe MOF	Mechanical coating	2 M $ZnSO_4$	22.6 mV (—)	4300 h (1, 1)	99.8%	69
	MOF-5W	Mechanical coating	2 M $ZnSO_4$	9.6 mV (1)	1000 h (5, 5)	99.7%	70
	ZIF-8	Drop casting and *in situ* growth	2 M $ZnSO_4$	—	1500 h (5, 5)	99.8%	71
	Zr_{12}-based 2D MOF	Drop casting	2 M $ZnSO_4$	17 mV (3)	2000 h (0.5, 0.5)	99%	72
	Co-ZIF-8	Electrosynthesis	2 M $ZnSO_4$	102.9 mV (1)	1280 h (1, 1)	98.4%	73
	Ti-based MOF (MIL-125(Ti))	Mechanical coating and *in situ* growth	2 M $ZnSO_4$	22 mV (1)	4200 h (1, 1)	99.8%	74
	A-ZIF-8	*In situ* spray coating	2 M $ZnSO_4$	32 mV (1)	1200 h (10, 1)	99.98%	75

performances. For example, the Zn@A-ZIF-8 symmetric cell showed a stable cycling performance of more than 1200 h even at an ultrahigh current density of 10 mA cm^{-2}. Also, Zn||Ti@A-ZIF-8 cells exhibited 99.98% of average CE along with 51 mV of voltage gap within 1000 cycles. These experimental results demonstrated that favourable electrolyte-anode interface modifications were made by A-ZIF-8: successful dendrite/HER suppression, fast Zn^{2+} conduction, and improved interfacial stability. Importantly, this modification process could extend beyond AZIBs and demonstrate wide applicability across various metal anodes such as Mg, Al, and Cu substrates, underscoring its broad versatility and practical relevance.

Recent research focused on MOF@Zn architectures prepared *via* facile and industry-friendly methods, aiming to enhance their commercial viability.[80,81] For example, W. W. Zhang *et al.*[70] used three types of MOFs (ZIF-7, MOF-5W, MOF-808), which underwent the same process of facile mechanical coating forming a MOF@Zn electrode. The only difference between the three electrodes was channel size (Fig. 3g). As a result, MOF-5W which had an appropriate channel size similar to $[Zn(H_2O)_6]^{2+}$, exhibited the most stable cycle performance as well as supremely improved CE. This is because the suitable channel size provided two different types of routes for Zn-ions to transfer: the confined channel space and the intergranular space. These dual-path transports enabled efficient Zn-ion transfer as well as effective desolvation of Zn^{2+}. However, if the channel size had been smaller or larger than it is supposed to be, anode corrosion and dendrite formation could have occurred due to inefficient or uncontrollable Zn-ion desolvation as well as direct contact between the electrolyte–anode interface. This is also clearly demonstrated in the following experimental results. The MOF-5W@Zn symmetric cell exhibited an impressive stable cycling performance of over 600 h compared to ZIF-7@Zn ($\sim$100 h) and MOF-808@Zn ($\sim$300 h) under 1 mA cm^{-2} and 1 mAh cm^{-2} conditions. Also, the MOF-5W@Zn||NVO full cell was shown to have a high CE of 99.7% which is significantly higher than that of other MOFs.

There were also approaches to grafting anode interface modification with the newest computer science technology: machine learning. J. B. Dong *et al.*[69] used a fully connected neural network (FCNN) model to select a promising MOF candidate from over 168 000 MOFs. This study utilized published sources to construct the database and performed machine learning analysis by assigning weights to ten parameters, including the number of valence electrons, largest and smallest cavity diameters, and void fraction. Through this process, a cerium-iron prussian blue analog (Ce–Fe MOF, $CeK[Fe(CN)_6]\cdot 4H_2O$) was selected and applied on Zn foil *via* a blade coating technique. The Ce–Fe MOF possessed appropriate ion-sieving channels, polar ligands, and zincophilic metals, which enabled selective ion transport, reduced the desolvation barrier, and promoted uniform Zn deposition. Also, polar cyano-ligands and zincophilic Ce atoms significantly influenced the dynamic conversion among $Zn(H_2O)_n^{2+}$, Zn^{2+}, and Zn metal. Consequently, the symmetric cell showed excellent cycling stability of 4300 h under 1 mA cm^{-2}, 1 mAh cm^{-2} conditions, which was about 50 times longer compared to bare Zn. Also, MOF@Zn||Cu exhibited an average CE of 99.8% during over 1400 cycles at 2 mA cm^{-2} and 1 mAh cm^{-2} conditions.

In conclusion, various types of MOFs can work harmoniously with Zn metal anodes by facilitating uniform ion deposition, suppressing side reactions, and stabilizing the interface. More specifically, MOFs with an appropriate pore size enable homogeneous Zn ion transport. Also, the coordination chemistry of MOF's metal nodes and organic linkers mediates critical side reactions. In addition, given the high prevalence of MOF-based interface modification in AZIB research, it can be concluded that AZIBs represent the most compatible battery platform for MOF-based interfacial engineering among various systems, such as LIBs and LMBs. Recent research on MOF-induced electrode modifications was mainly about AZIBs, focusing on MOFs' channel size and surface chemistry.

4. Separator modification using MOFs

The separator acts as a physical barrier between the cathode and anode, playing a vital role in facilitating ion transport and preventing short circuits in the battery.[82] Typically, separators are constructed with a porous structure containing numerous micropores that serve as channels for ion migration between electrodes. This well-designed porosity ensures efficient ionic conduction, contributing to stable cycling performance and high battery efficiency during battery cycling.

Without a separator, the cathode and anode come into direct contact, and a low-resistance path for carrier ions forms, which could cause an internal short circuit. This problem can cause undesirable high current flow, which can lead to localized overheating, performance degradation, and serious safety hazards including ignition or explosion. Positioned between the electrodes, the separator functions as an electrical insulator, preventing electrical failure while maintaining sufficient ionic conductivity.

Although interface regulations in batteries are primarily discussed in the context of electrode materials, conventional separators can also suffer from partial interface issues (Fig. 4a). In LIBs, a critical issue is the insufficient penetration of the electrolyte into the separator. The poor wettability of the separator surface, because of its low electrolyte affinity and weak interactions, restricts the formation of effective ion transport paths.[83–85] In LSBs, the shuttle effect, which refers to the undesirable migration of soluble LiPSs (Li_2S_n, $4 \leq n < 8$) between the electrodes, leads to continuous loss of active sulfur and rapid capacity fading.[86,87] In AZIBs, uncontrolled dendrite growth and side reactions cause significant challenges such as degradation of the separator. MOFs can address each of these issues by enhancing electrolyte uptake, and facilitating the conversion of intermediate products, and promoting uniform ion transport.[4,88] This strategy provides a promising approach to overcome the major drawbacks of conventional commercial separators through surface modification.

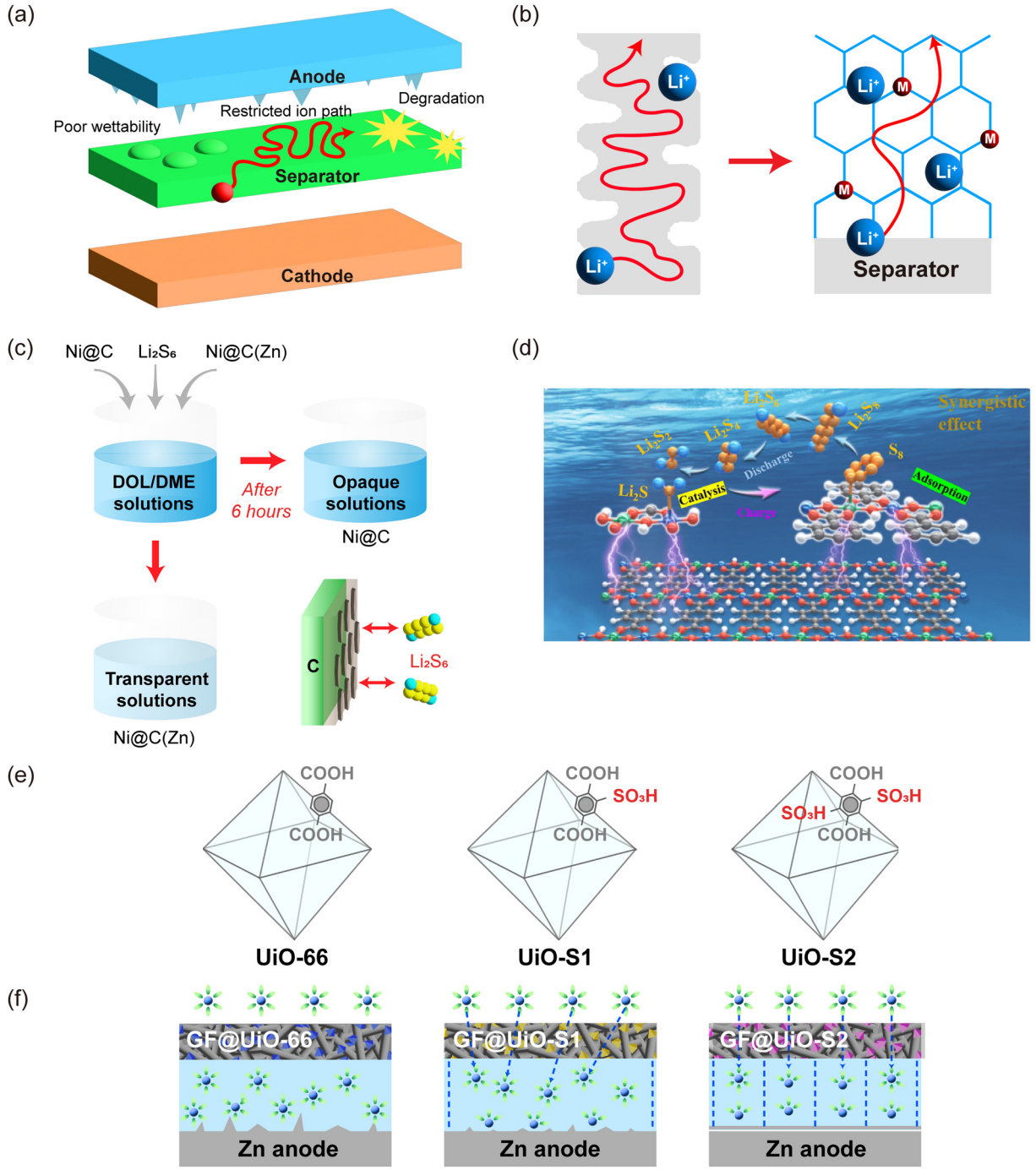

Fig. 4 (a) Schematic illustration of separator-related interfacial issues in batteries. (b) Li^+ transport in a conventional separator *versus* a MOF-based separator of LIB with OMSs. (c) Illustration of Li_2S_6 adsorption in Ni@C and Ni@C(Zn) solutions, highlighting completely transparent Ni@C(Zn) solution. (d) Illustration of the synergistic adsorption and catalytic effects on polysulfide regulation in Li–S batteries. Adapted from ref. 97 with permission from Journal of Energy Chemistry, Copyright 2025. (e) Structures of GF@UiO-66, GF@UiO-S1, and GF@UiO-S2. (f) Dendrite suppression on Zn anodes with various GF-based materials (UiO-66, UiO-S1, and UiO-S2) in AZIBs.

4.1. Modification of LIB separators using MOFs

To address the insufficient electrolyte wettability of polypropylene (PP) separators in LIBs, X. Li *et al.*[85] introduced a surface engineering approach—hydrothermal method—using chromium-based MOFs (Cr-MOFs), specifically MIL-88B(Cr) and MIL-101(Cr). Both MOFs had a common Cr^{3+} metal center and organic linker (1,4-benzenedicarboxylate), but exhibited notable differences in morphology, Brunauer–Emmett–Teller (BET) surface area, and total pore volume with MIL-101(Cr) having significantly larger internal surface area and porosity. These structural differences were reflected in enhanced electrolyte uptake. MIL-101(Cr)/PP showed

superior electrolyte uptake, which was further enhanced in a thicker separator—MIL-101(Cr)/PP-1—, indicating the role of high porosity and increased volume in retaining electrolyte. From an electrochemical performance aspect, MOF-coated separators—especially MIL-101(Cr)/PP-2—exhibited superior ionic conductivity due to their abundant pores, open metal sites (OMSs), and rate capability compared to PP. In particular, the thinner MIL-101(Cr)/PP-2 provided a shorter ion transport path, contributing to its enhanced performance, resulting in 56.2% capacity retention at 10C (Fig. 4b).[89]

Similarly, M. Li *et al.*[90] addressed the ion transport constraints of LIB separators by directly constructing a MOF layer on a PVDF membrane through *in situ* interfacial synthesis of HKUST-1, a Cu-BTC-type MOF. Using a superspreading strategy under ambient temperature, HKUST-1 was uniformly grown within the membrane, forming *sub*-nanometer channels and OMSs that facilitated fast and uniform Li ion transport. The resulting MOF layer exhibited a continuous and dense morphology, with vertically aligned growth that densely filled the uniform pores of the PVDF membrane. Compared to a commercial PP membrane, the resulting PVDF-MOF composite membrane showed markedly improved electrolyte wettability, along with higher porosity and electrolyte uptake. The PVED-MOF separator showed markedly improved ionic conductivity (134.6% increase), lower resistance (1.89 Ω), and superior thermal stability compared to PP. The presence of the MOF layer also regulated Li^+ flux uniformly and suppressed dendrite formation, enabling the cell to retain 87.5% of its initial capacity at 2C, with a CV peak current of 0.89 mA cm^{-2} and a wider stability window (2.5–4.5 V).

Recently, J. Li *et al.*[91] developed a fluorinated MOF-based separator (UIO-66-F@PP) to enhance both the electrochemical performance and safety of LIBs. In this work, fluorine (F) functionalized UIO-66 (UIO-66-F) was synthesized by grafting highly electronegative and polarizable –F groups onto Zr-based UIO-66.[92] The resulting MOF was coated onto both sides of a commercial PP separator to fabricate a composite structure. In burning tests, UIO-66-F@PP exhibited rapid self-extinguishing within 2 s due to the shielding effect of F and strong C–F bonds, confirming its improved thermal stability. The hydrophilic –F groups and porous MOF structure reduced interfacial resistance, contributing to enhanced electrolyte affinity. Notably, UIO-66-F@PP effectively suppressed dendrite formation, possessing a high Li transference number. The cell retained 84.8% of its capacity at 1C, and the CV indicated fast and reversible kinetics of the modified separator.

MOF-coated separators enhance Li^+ transport by providing abundant pores and OMSs that improve electrolyte wettability and lower interfacial resistance, supported further by the introduction of specific metal centers and functional groups. MOFs' hierarchical pore structures and nanoscale channels promote uniform ion flux, preventing localized depletion and dendrite formation. Together, these interfacial features improve ion conductivity, rate performance, and overall electrochemical stability in LIBs.

4.2. Modification of next generation battery separators using MOFs

LSBs are limited by the shuttle effect caused by the dissolution and migration of intermediate PS, leading to severe capacity fading and reduced cycle stability.[93] To mitigate these issues, J. Cheng *et al.*[94] synthesized a magnetic porous Ni–C composite (Ni@C(Zn)) using a Ni–Zn bimetallic MOF as the precursor, and coated it on one side of a commercial polyethylene (PE) separator to suppress the shuttle effect. To contrast its improvement, this work compared Ni@C(Zn) with a Ni@C modified separator. Ni-MOF and Zn-MOF were selected based on previous reports highlighting their successful integration with carbon materials, which enabled excellent electrical conductivity and efficient control of PS.[95,96] Ni@C(Zn) exhibited a sheet-like layered microsphere morphology with uniformly dispersed Ni nanoparticles and abundant micro/mesopores, formed by Zn sublimation during carbonization. Moreover, its sharper and more intense X-ray diffraction peaks indicate higher crystallinity and improved structural stability compared to Ni@C. To evaluate the adsorption capability, both Ni@C(Zn) and Ni@C were dispersed in DOL/DME solutions containing an equal amount of Li_2S_6. The solution containing Ni@C(Zn) became completely transparent, in contrast to the Ni@C containing solution, indicating that Li_2S_6 was fully adsorbed (Fig. 4c). This result confirmed the superior PS adsorption capability of the Ni@C(Zn) composites. Furthermore, CV showed enhanced PS redox kinetics with a narrowed voltage gap (0.31 V) by implying their reduction in electrochemical polarization and the suppression of side reactions. Ni@C(Zn) also exhibited higher current density and lower resistance (41.986 Ω), indicating improved Li^+ diffusion attributed to superior wettability.

In a related study, X. Leng *et al.*[97] also employed a Ni-based composite to simultaneously achieve PS confinement and catalytic conversion (Fig. 4d). Using electrospinning, they fabricated a nanocomposite polyacrylonitrile (PAN) based separator (NCMP) coated with bimetallic Ni–Co MOF nanoparticles. The resulting MOF displayed a sea-urchin-like morphology with needle-shaped nanorods. The Ni–Co MOF, featuring a porous microspherical architecture and abundant active metal sites, exhibited strong affinity for PS species. Notably, the Ni and Co centers provided the highest binding energies with PS, effectively preventing their diffusion across the separator. The PAN nanofiber matrix served as a robust scaffold for MOF dispersion, facilitating electrolyte infiltration and Li^+ transport while selectively suppressing PS migration. Galvanostatic tests showed the NCMP separator achieved 1457 mAh g^{-1} upon returning to 0.1C from 10C and retained 794 mAh g^{-1} (84.1%) over 500 cycles, substantially outperforming bare Celgard.

More recently, H. Zhu *et al.*[98] proposed a modified separator based on a Ni-doped ZIF-67 structure coated with polydopamine (PDA), followed by carbonization and phosphorization to yield a NiCoP@NC composite. This material was applied to a commercial PP (Celgard 2500) separator. The resulting NiCoP@NC composite exhibited a slightly wrinkled rhombohedral dodecahedron

morphology with surface-decorated nanoparticles. Remarkably, the structure was maintained even after thermal treatment at 600 °C, owing to the protective PDA layer. NiCoP was uniformly coated onto the porous PP surface and featured intrinsically high polarity, enabling strong adsorption of LiPSs. The coating layers also exhibited excellent mechanical integrity and flexibility, ensuring long-term stability against PS permeation. The NiCoP@NC-modified separator exhibited improved electrolyte wettability compared to bare PP. Cell evaluation results showed that NiCoP@NC-modified cells retained 71.23% capacity over 300 cycles. To further evaluate the catalytic activity, symmetric cell was assembled, and CV revealed a higher current response, better reversibility, and faster LiPS redox kinetics than NiCo@C. Common MOF-based separator designs include introducing active metal sites for PS, constructing a porous channel for regulated Li^+ flux, and integrating bimetallic composites or doping conductive metals to suppress shuttle-induced side reactions. Collectively, these MOF-enabled interfacial architectures demonstrate a robust approach to improving ionic conductivity, redox reversibility, and long-term cycling stability, highlighting their potential for next-generation high-performance LSBs.

AZIBs faced restricted practical application due to side reactions—such as Zn dendrite formation and HERs—that compromise long-term stability.[99] To address these issues, R. Chen *et al.*[100] proposed a modified separator by coating a glass fiber (GF) membrane with UiO-S2, a Zr-based MOF derived from UiO-66 through oxidation after the introduction of thiol (-SH) groups.[99] The resulting GF@UiO-S2 separator was designed to regulate Zn ion flux and suppress parasitic reactions. UiO-S2 contained two sulfonic acid ($-SO_3H$) groups, which exhibited strong affinity toward Zn^{2+}, enabling uniform ion distribution and facilitating 3D nucleation near adsorption sites. This led to the formation of a smooth and dense Zn layer, while the accelerated desolvation kinetics suppressed the HER and corrosion. For comparison, additional separators were fabricated using UiO-66 and a mono-functionalized UiO-S1 (with one $-SO_3H$ group), but neither matched the performance of GF@UiO-S2 with two $-SO_3H$ groups (Fig. 4e and f). These results highlighted a strong correlation between the number of $-SO_3H$ groups and the suppression of dendritic growth. GF@UiO-S2 showed excellent stability and reversibility in Zn cells, with low polarization (48 mV) and nucleation overpotential (46 mV), nearly 100% CE over 100 cycles, confirming uniform nucleation and high reversibility. It also exhibited high ionic conductivity (22.00 mS cm^{-1}), emphasizing the role of SO_3H groups in ion transport.

In another study, N. Maeboonruan *et al.*[101] explored the use of MOF-modified separators to achieve homogeneous Zn ion flux and mitigate dendrite growth. They deposited MOF-808 (zirconium(IV)-based MOF with 1,3,5-benzenetricarboxylic acid (H_3BTC) linkers) and ZIF-8 ($Zn(MeIM)_2$, MeIM: 2-methylimidazolate) onto GF membranes *via* dip coating. MOF-808 featured both micropores and mesopores with particle sizes below 100 nm, while ZIF-8 possessed only micropores and was slightly larger (~200 nm). BET measurements confirmed that MOF-808 has a higher surface area and pore volume than ZIF-8. MOF-modified separators increased current density during Zn deposition, promoting uniform Zn layers with suppressed dendrites.[102] They also retained 63.9% (MOF-808@GF) and 56.7% (ZIF-8@GF) capacity after 20000 cycles.

More recently, Z. He *et al.*[4] developed a functionalized separator using NM-125, an amino ($-NH_2$)-modified MIL-125 (Ti-based MOF), which was *in situ* loaded onto a GF membrane to form NM-125-GF. Compared to pristine MIL-125, NM-125 exhibited a smaller particle size (~200 nm), narrower pore size (0.495 nm), and a larger BET surface area (925.2 m^2 g^{-1}), allowing for uniform dispersion within the separator matrix. The polar $-NH_2$ groups served as Zn^{2+} affinitive sites, promoting homogeneous ion flux and enhancing desolvation kinetics, thereby effectively suppressing dendrite growth and the HER. NM-125-GF promoted uniform Zn^{2+} transport, suppressed byproducts derived by $-NH_2$ groups' inhibiting role. Furthermore, the assembled symmetric cell showed high exchange current density (15.07 mA cm^{-2}), and the Zn||MnO_2 cell indicated an initial capacity of 160.2 mA g^{-1} and retained 99.8% capacity over 700 cycles.[103] These confirmed the outstanding stability and effectiveness of modified separators.

In AZIB systems, recent separator designs highlight the importance of chemical functionality within MOF coatings for directing stable Zn deposition. By mitigating the HER and other undesired pathways, these tailored interfacial environments enhance electrochemical performance and cycling longevity, positioning functionalized MOFs as a promising platform for next-generation AZIB separators.

Conclusions

In general, MOFs have been widely used to modify various types of batteries (LIBs, LMBs, LSBs, AZIBs, *etc.*) due to the broad tunability of their porous structures, large surface areas, and polar ligands. These features enable MOFs to regulate ion transport, suppress critical side reactions, and stabilize electrode–electrolyte as well as separator–electrolyte interfaces, all of which are critical for enhancing battery performance and lifespan. Therefore, this review aims to highlight key difficulties, summarize important previous studies, and provide insights into the future research directions (Fig. 5).

In LIBs, MOFs are strategically utilized in multiple cell components (anode, cathode, and separator), to address specific performance and stability challenges. For instance, the cathode showed improved interfacial stability and electrochemical performance through hybrid designs, c-MOFs, and i-MOF layers capable of inserting Li ions. In the anode, the MOF precursor was used *via* heat treatment to easily form the Li ion diffusion channels and mitigate volume expansion. Moreover, enhancing thermal stability and interfacial kinetics of separators by using MOFs added with a halogen(–F) functional group was shown.

For next-generation batteries, interfacial modifications play a critical role in determining the commercial viability of the battery. In LSBs, MOF-based cathode modification strategies

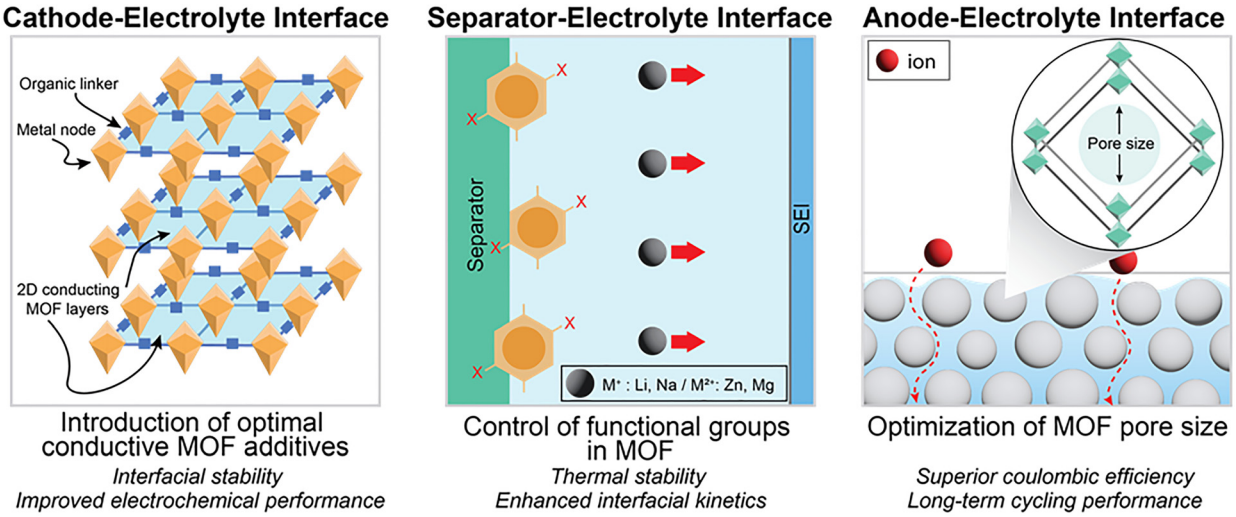

Fig. 5 Schematic illustration of solution methods for interfacial issues and description of improvements in battery components: cathode, anode, and separator.

such as chemically anchoring sulfur species or constructing conductive MOF composites, are employed to inhibit sulfur release and alleviate the shuttle effect. Also, bimetallic MOFs, derived by integrating two different MOFs have been applied to separator modification, enabling complex functional performance, which overall enhances catalytic effectiveness and thermal stability. Moreover, in LMBs, anode modification using MOFs that serve as an artificial SEI layer promotes uniform Li nucleation and suppresses dendrite formation, thereby improving electrochemical performance as well as cell stability.

Among all these systems, MOF based modification is particularly active in AZIBs, owing to the hydrophilicity and electrochemical stability of MOFs under low-voltage conditions. For example, in the cathode, 2D conductive and hybrid MOF designs are applied to enhance structural stability and performance limitations. Likewise, modifying the Zn anode with pore-optimized MOFs improved CE, long-term cycling performance, and interfacial stability. Besides, maximizing the functionality of MOFs in the separator is used to treat dendrites by enabling a uniform Zn ion flux.

As shown above, research on battery modification using MOFs has been successfully conducted. However, the experimental procedures remain complex, and the practical applicability is still limited. Moreover, synthesizing novel MOFs and identifying suitable candidates often requires extensive trial-and-error processes. Therefore, machine learning is expected to play an important role in screening effective MOFs for battery applications. A key challenge in this approach lies in designing the machine learning model, particularly in determining which parameters should be considered and given more weight value during the MOF selection process.

Previous studies have applied parameters such as the number of valence electrons, cavity diameters, and void fraction of metal ions and linkers. Each parameter is critical, as it influences the selection of metal nodes, linkers, and the electrostatic interactions between them. Even with the same set of parameters, varying their weights—or modifying the parameters themselves to achieve specific goals—can lead to diverse MOF candidates, highlighting the great potential for machine learning based studies in battery applications. The incorporation of machine learning offers significant advantages, including the reduction of trial-and-error processes and the improved capability to screen for low-cost, easily synthesizable MOF candidates. All things considered, this synergy is expected to open new frontiers in battery interface modification and thereby accelerate the development of high-performance, next-generation energy storage technologies.

Conflicts of interest

There are no conflicts to declare.

Data availability

No primary research results, software or code have been included and no new data were generated or analysed as part of this review.

Acknowledgements

This work was supported by the National Research Foundation of Korea (NRF) grant funded by the Korea government (MSIT) (No. RS-2022-NR071869 and RS-2025-02215502). This work was supported by the National Research Foundation of Korea (NRF) grant funded by the Korea government (MSIT and MOE) (No. RS-2025-16063688).

Notes and references

1 J. Li, B. Wang, S. Wang, W. Li and D. Chen, *ChemSusChem*, 2025, **18**, e202401217.

2 Y. Song, L. Wang, L. Sheng, D. Ren, H. Liang, Y. Li, A. Wang, H. Zhang, H. Xu and X. He, *Energy Environ. Sci.*, 2023, **16**, 1943–1963.
3 Y. H. Lee, Y. Jeoun, J. H. Kim, J. Shim, K. S. Ahn, S. H. Yu and Y. E. Sung, *Adv. Funct. Mater.*, 2024, **34**, 2310884.
4 Z. He, X. Zhu, Y. Song, B. Li, X. Xu, Z. Zhang, N. Zhao, Y. Liu, J. Zhu, L. Wang, L. Dai and H. Tian, *Energy Storage Mater.*, 2025, **74**, 103886.
5 J. Cho, Y. J. Kim and B. Park, *Chem. Mater.*, 2000, **12**, 3788–3791.
6 Y. Li, X. Liu, D. Ren, H. Hsu, G.-L. Xu, J. Hou, L. Wang, X. Feng, L. Lu, W. Xu, Y. Ren, R. Li, X. He, K. Amine and M. Ouyang, *Nano Energy*, 2020, **71**, 104643.
7 F. Schipper, H. Bouzaglo, M. Dixit, E. M. Erickson, T. Weigel, M. Talianker, J. Grinblat, L. Burstein, M. Schmidt, J. Lampert, C. Erk, B. Markovsky, D. T. Major and D. Aurbach, *Adv. Energy Mater.*, 2018, **8**, 1701682.
8 A. A. Assegie, J. H. Cheng, L. M. Kuo, W. N. Su and B. J. Hwang, *Nanoscale*, 2018, **10**, 6125–6138.
9 L. T. Hieu, S. So, I. T. Kim and J. Hur, *Chem. Eng. J.*, 2021, **411**, 128584.
10 K. Namsheer. and C. S. Rout, *RSC Adv.*, 2021, **11**, 5659–5697.
11 X. Huang, Z. Zeng, Z. Fan, J. Liu and H. Zhang, *Adv. Mater.*, 2012, **24**, 5979–6004.
12 Z. Xiong, Y. S. Yun and H. J. Jin, *Materials*, 2013, **6**, 1138–1158.
13 C. W. Park, J. H. Lee, J. K. Seo, W. Y. Jo, D. Whang, S. M. Hwang and Y. J. Kim, *Nat. Commun.*, 2021, **12**, 2145.
14 X. Zhao, Y. Wang, D. S. Li, X. Bu and P. Feng, *Adv. Mater.*, 2018, **30**, e1705189.
15 H. Li, M. Eddaoudi, M. O'Keeffe and O. M. Yaghi, *Nature*, 1999, **402**, 276–279.
16 Q. Zeng, R. Zhang, H. Lu, J. Yang, J. Rong, J. Weng, B. Zhang, S. Xiong, Q. Zhang and S. Huang, *Energy Environ. Sci.*, 2025, **18**, 1343–1353.
17 T. Yang, R. Xiao, F. Lu, X. Ke, M. Wang and K. Wang, *New J. Chem.*, 2025, **49**, 6674–6683.
18 L. Jiang, Y. Dong, Y. Yuan, X. Zhou, Y. Liu and X. Meng, *Chem. Eng. J.*, 2022, **430**, 132823.
19 Y. Peng, J. Xu, J. Xu, J. Ma, Y. Bai, S. Cao, S. Zhang and H. Pang, *Adv. Colloid Interface Sci.*, 2022, **307**, 102732.
20 S. Nagappan, M. Duraivel, V. Elayappan, N. Muthuchamy, B. Mohan, A. Dhakshinamoorthy, K. Prabakar, J.-M. Lee and K. H. Park, *Energy Technol.*, 2023, **11**, 2201200.
21 J. Xu, *Nano-Micro Lett.*, 2022, **14**, 166.
22 W. P. Wang, J. Zhang, J. Chou, Y. X. Yin, Y. You, S. Xin and Y. G. Guo, *Adv. Energy Mater.*, 2020, **11**, 2000791.
23 C. Xu, B. Li, H. Du and F. Kang, *Angew. Chem., Int. Ed.*, 2012, **51**, 933–935.
24 M. Wang, X. Zheng, X. Zhang, D. Chao, S. Z. Qiao, H. N. Alshareef, Y. Cui and W. Chen, *Adv. Energy Mater.*, 2020, **11**, 2002904.
25 F. Wang, E. Hu, W. Sun, T. Gao, X. Ji, X. Fan, F. Han, X. Q. Yang, K. Xu and C. Wang, *Energy Environ. Sci.*, 2018, **11**, 3168–3175.
26 R. Konar, S. Maiti, B. Markovsky, H. Sclar and D. Aurbach, *Chem.:-Methods*, 2023, **4**, e202300039.
27 J. Lin, C. Zeng, Y. Chen, X. Lin, C. Xu and C.-Y. Su, *J. Mater. Chem. A*, 2020, **8**, 6607–6618.
28 C. Huang, Z. Wang, Z.-Q. Fang, S.-X. Zhao and L.-J. Ci, *J. Power Sources*, 2021, **499**, 229967.
29 Z. Wu, D. Adekoya, X. Huang, M. J. Kiefel, J. Xie, W. Xu, Q. Zhang, D. Zhu and S. Zhang, *ACS Nano*, 2020, **14**, 12016–12026.
30 S. Shin, Y. Yoon, S. Park and M. Whan Shin, *Appl. Surf. Sci.*, 2024, **643**, 158735.
31 Q. Jiang, P. Xiong, J. Liu, Z. Xie, Q. Wang, X. Q. Yang, E. Hu, Y. Cao, J. Sun, Y. Xu and L. Chen, *Angew. Chem., Int. Ed.*, 2020, **59**, 5273–5277.
32 M. Yang, Y. Wang, Y. F. Huang, J. M. Xiao, G. Y. Zhu, Y. Fang, X. C. Zhou, J. H. Long, M. Xie, D. S. Bin and D. Li, *Angew. Chem., Int. Ed.*, 2025, **64**, e202421008.
33 Q. Zhu, W. Sun, H. Zhou and D. Mao, *Batteries*, 2025, **11**, 89.
34 Y. Feng, Y. Zhang, G. Du, J. Zhang, M. Liu and X. Qu, *New J. Chem.*, 2018, **42**, 13775–13783.
35 Y. Xie, J. Cao, X. Wang, W. Li, L. Deng, S. Ma, H. Zhang, C. Guan and W. Huang, *Nano Lett.*, 2021, **21**, 8579–8586.
36 P. Shi, C. Zhu, C. Chen, Y. Luo, F. Sun, X. Du, T. Zhou and G. Gao, *Carbon Future*, 2025, **2**, 9200035.
37 S. O. Ajayi, T. H. Dolla, L. L. Sikeyi, A. O. Akinola, W. K. Maboya, X. Liu, P. R. Makgwane and M. K. Mathe, *Mater. Today Sustainability*, 2024, **27**, 100899.
38 K. W. Nam, S. S. Park, R. Dos Reis, V. P. Dravid, H. Kim, C. A. Mirkin and J. F. Stoddart, *Nat. Commun.*, 2019, **10**, 4948.
39 C. Yin, C. Pan, Y. Pan and J. Hu, *J. Colloid Interface Sci.*, 2023, **642**, 513–522.
40 W. Wang, Z. Gao, L. Cao, L. Xu, N. Yu, M. Li, F. Wei, Y. Sui, L. Li and L. Zhang, *J. Electroanal. Chem.*, 2024, **952**, 117994.
41 M. Jiang, Q. Qin, J. Li and M. Zeng, *ACS Appl. Mater. Interfaces*, 2025, **17**, 13997–14007.
42 D. Kundu, B. D. Adams, V. Duffort, S. H. Vajargah and L. F. Nazar, *Nat. Energy*, 2016, **1**, 16119.
43 D. Jia, Z. Shen, Y. Lv, Z. Chen, H. Li, Y. Yu, J. Qiu and X. He, *Adv. Funct. Mater.*, 2023, **34**, 2308319.
44 Y. Zhang, Z. Li, B. Zhao, Z. Wang and J. Liu, *J. Mater. Chem. A*, 2024, **12**, 1725–1735.
45 X. Wu, C. Yin, M. Zhang, Y. Xie, J. Hu, R. Long, X. Wu and X. Wu, *Chem. Eng. J.*, 2023, **452**, 139573.
46 X. Ma, K. Han, H. Li, L. Song, Y. Lin, L. Lin, Y. Liu, Y. Zhao, Z. Yang and W. Huang, *Energy Environ. Sci.*, 2025, **18**, 897–909.
47 K. Xu, *Chem. Rev.*, 2004, **104**, 4303–4418.
48 K. Xu, *Chem. Rev.*, 2014, **114**, 11503–11618.
49 J. W. Sturman, M. S. E. Houache, W. D. do Pim, E. A. Baranova, M. Murugesu and Y. Abu-Lebdeh, *ACS Appl. Energy Mater.*, 2023, **7**, 21–30.
50 E. Peled and S. Menkin, *J. Electrochem. Soc.*, 2017, **164**, A1703–A1719.
51 P. Verma, P. Maire and P. Novák, *Electrochim. Acta*, 2010, **55**, 6332–6341.
52 L. Sun, Y. Liu, R. Shao, J. Wu, R. Jiang and Z. Jin, *Energy Storage Mater.*, 2022, **46**, 482–502.
53 S. Mamidi, D. Potphode, A. D. Pathak and C. S. Sharma, *Adv. Energy Sustainability Res.*, 2021, **2**, 2100102.
54 Y. Yang, M. Li and X. Hu, *Molecules*, 2024, **29**, 3566.
55 Y. Han, P. Qi, J. Zhou, X. Feng, S. Li, X. Fu, J. Zhao, D. Yu and B. Wang, *ACS Appl. Mater. Interfaces*, 2015, **7**, 26608–26613.
56 L. Zhang, Y. Lin, X. Peng, M. Wu and T. Zhao, *ACS Appl. Mater. Interfaces*, 2022, **14**, 24798–24805.
57 Y. Y. Chen, M. Y. Huang, G. F. Deng, C. L. Wu, H. Zhong, A. Zeb, X. M. Lin, Y. B. Wu, Z. Y. Wu, Z. G. Xu and Y. P. Cai, *Chem. Eng. J.*, 2024, **486**, 150111.
58 S. Y. Bai, Y. Sun, J. Yi, Y. B. He, Y. Qiao and H. S. Zhou, *Joule*, 2018, **2**, 2117–2132.
59 X. B. Cheng, R. Zhang, C. Z. Zhao and Q. Zhang, *Chem. Rev.*, 2017, **117**, 10403–10473.
60 W. Xu, J. Wang, F. Ding, X. Chen, E. Nasybulin, Y. Zhang and J.-G. Zhang, *Energy Environ. Sci.*, 2014, **7**, 513–537.
61 B. Li, Y. Chao, M. Li, Y. Xiao, R. Li, K. Yang, X. Cui, G. Xu, L. Li, C. Yang, Y. Yu, D. P. Wilkinson and J. Zhang, *Electrochem. Energy Rev.*, 2023, **6**, 7.
62 Z. Yu, D. G. Mackanic, W. Michaels, M. Lee, A. Pei, D. Feng, Q. Zhang, Y. Tsao, C. V. Amanchukwu, X. Yan, H. Wang, S. Chen, K. Liu, J. Kang, J. Qin, Y. Cui and Z. Bao, *Joule*, 2019, **3**, 2761–2776.
63 T. Zhou, J. D. Shen, Z. S. Wang, J. Liu, R. Z. Hu, L. Z. Ouyang, Y. Z. Feng, H. Liu, Y. Yu and M. Zhu, *Adv. Funct. Mater.*, 2020, **30**, 1909159.
64 J. Ding, T. Du, L. R. Jensen, S. S. Sorensen, D. Wang, S. Wang, L. Zhang, Y. Yue and M. M. Smedskjaer, *Adv. Mater.*, 2024, **36**, e2400652.
65 L. Kong, Y. Li, C. Peng, Z. Zhao, J. Xiao, Y. Zhao and W. Feng, *Nat. Commun.*, 2025, **16**, 1885.
66 Y. Zhang, T. Zhan, M. Zhu and L. Qi, *Small Methods*, 2025, **9**, 2402213.
67 Z. X. Ou, X. Li, Y. Wang, D. X. He, W. Gan and Q. H. Yuan, *Electrochim. Acta*, 2025, **523**, 145987.
68 D. Li, J. Long, X. Liu, X. Chen, Z. Li and G. Lei, *Energy Fuels*, 2025, **39**, 8742–8752.
69 J. Dong, G. Zhou, W. Ding, J. Ji, Q. Wang, T. Wang, L. Zhang, X. Zou, J. Yin and E. H. Ang, *Energy Environ. Sci.*, 2025, **18**, 4872–4882.
70 W. W. Zhang, W. T. Qi, K. Yang, Y. Y. Hu, F. Y. Jiang, W. B. Liu, L. Y. Du, Z. H. Yan and J. C. Sun, *Energy Storage Mater.*, 2024, **71**, 103616.

71 Y. M. Xu, X. S. Li, X. T. Wang, Q. J. Weng and W. J. Sun, *J. Power Sources*, 2024, **624**, 235525.
72 L. Lei, B. Zhao, X. Pei, L. Gao, Y. Wu, X. Xu, P. Wang, S. Wu and S. Yuan, *ACS Appl. Mater. Interfaces*, 2024, **16**, 485–495.
73 Z. Jiang, Z. Du, R. Pan, F. Cui, G. Zhang, S. Lei, G. He, K. Yin and L. Sun, *Adv. Energy Mater.*, 2024, **14**, 2402150.
74 D. Y. Xiong, L. Yang, Z. W. Cao, F. R. Li, W. T. Deng, J. G. Hu, H. S. Hou, G. Q. Zou and X. B. Ji, *Adv. Funct. Mater.*, 2023, **33**, 2301530.
75 Y. Xiang, L. Zhou, P. Tan, S. Dai, Y. Wang, S. Bao, Y. Lu, Y. Jiang, M. Xu and X. Zhang, *ACS Nano*, 2023, **17**, 19275–19287.
76 B. Niu, J. Wang, Y. Guo, Z. Li, C. Yuan, A. Ju and X. Wang, *Adv. Energy Mater.*, 2024, **14**, 2303967.
77 W. Du, E. H. Ang, Y. Yang, Y. Zhang, M. Ye and C. C. Li, *Energy Environ. Sci.*, 2020, **13**, 3330–3360.
78 B. Lee, M. G. Son, S. A. Song, K. Kim, J. Y. Woo, Y. Choa, J. Kang and S. N. Lim, *J. Colloid Interface Sci.*, 2025, **680**, 640–650.
79 X. Pu, B. Jiang, X. Wang, W. Liu, L. Dong, F. Kang and C. Xu, *Nano-Micro Lett.*, 2020, **12**, 152.
80 Y. Xing, K. Feng, C. Kong, G. Wang, Y. Pei, Q. Huang and Y. Liu, *Coatings*, 2023, **13**, 1457.
81 D. Chakraborty, A. Yurdusen, G. Mouchaham, F. Nouar and C. Serre, *Adv. Funct. Mater.*, 2023, **34**, 2309089.
82 Y. Sun, Y. Zhang, Z. Chen, C. Li, C. Duan, S. Kawi and Y. Li, *J. Colloid Interface Sci.*, 2025, **683**, 262–273.
83 C. F. J. Francis, I. L. Kyratzis and A. S. Best, *Adv. Mater.*, 2020, **32**, e1904205.
84 Z. Liu, Y. Jiang, Q. Hu, S. Guo, L. Yu, Q. Li, Q. Liu and X. Hu, *Energy Environ. Mater.*, 2020, **4**, 336–362.
85 X. Li, F. Zhang, M. Zhang, Z. Zhou and X. Zhou, *J. Energy Storage*, 2023, **59**, 106473.
86 M. A. Al-Tahan, B. Miao, S. Xu, M. Hou, M. R. Shatat, M. Asad, Y. Luo, A. E. Shrshr and J. Zhang, *Colloids Surf., A*, 2024, **682**, 132899.
87 S. Lin, J. Dong, R. Chen, G. Zhang, T. Huang, J. Li, H. Zhou, L.-H. Chung, X. Hu and J. He, *J. Alloys Compd.*, 2023, **965**, 171389.
88 Y. Li, X. Peng, X. Li, H. Duan, S. Xie, L. Dong and F. Kang, *Adv. Mater.*, 2023, **35**, e2300019.
89 B. M. Wiers, M. L. Foo, N. P. Balsara and J. R. Long, *J. Am. Chem. Soc.*, 2011, **133**, 14522–14525.
90 M. Li, S. Cheng, J. Zhang, C. Huang, J. Gu, J. Han, X. Xu, X. Chen, P. Zhang and Y. You, *Chem. Eng. J.*, 2024, **487**, 150709.
91 J. Li, G. Yin, Y. Wang, Y. Xiang, N. Yu, X. Li, Y. Jiang, M. Xu and X. Zhang, *Chem. Eng. J.*, 2025, **507**, 160148.
92 Y. Wang, Z. Wu, F. M. Azad, Y. Zhu, L. Wang, C. J. Hawker, A. K. Whittaker, M. Forsyth and C. Zhang, *Nat. Rev. Mater.*, 2023, **9**, 119–133.
93 S. Bai, X. Liu, K. Zhu, S. Wu and H. Zhou, *Nat. Energy*, 2016, **1**, 16094.
94 J. Cheng, Y. Wang, X. Qian, L. Jin, J. Chen, Q. Hao and K. Zhang, *J. Alloys Compd.*, 2023, **935**, 168066.
95 D. H. Lee, J. H. Ahn, M.-S. Park, A. Eftekhari and D.-W. Kim, *Electrochim. Acta*, 2018, **283**, 1291–1299.
96 M. Rana, J. Kim, L. Peng, H. Qiu, R. Kaiser, L. Ran, M. S. A. Hossain, B. Luo, I. Gentle, L. Wang, R. Knibbe and Y. Yamauchi, *Nanoscale*, 2021, **13**, 11086–11092.
97 X. Leng, J. Zeng, M. Yang, C. Li, S. V. P. Vattikuti, J. Chen, S. Li, J. Shim, T. Guo and T. J. Ko, *J. Energy Chem.*, 2023, **82**, 484–496.
98 H. Zhu, S. Dong, J. Xiong, P. Wan, X. Jin, S. Lu, Y. Zhang and H. Fan, *J. Colloid Interface Sci.*, 2023, **641**, 942–949.
99 R. Li, B. Yan, Z. Chen, Z. He and J. Yang, *J. Energy Chem.*, 2025, **105**, 860–868.
100 R. Chen, G. Zhang, H. Zhou, J. Li, J. Li, L. H. Chung, X. Hu and J. He, *Small*, 2024, **20**, e2305687.
101 N. Maeboonruan, J. Lohitkarn, C. Poochai, A. Tuantranont, P. Limthongkul and C. Sriprachuabwong, *J. Energy Storage*, 2024, **85**, 111063.
102 Z. Zhao, J. Zhao, Z. Hu, J. Li, J. Li, Y. Zhang, C. Wang and G. Cui, *Energy Environ. Sci.*, 2019, **12**, 1938–1949.
103 Y. Su, B. Liu, Q. Zhang, J. Peng, C. Wei, S. Li, W. Li, Z. Xue, X. Yang and J. Sun, *Adv. Funct. Mater.*, 2022, **32**, 2204306.

